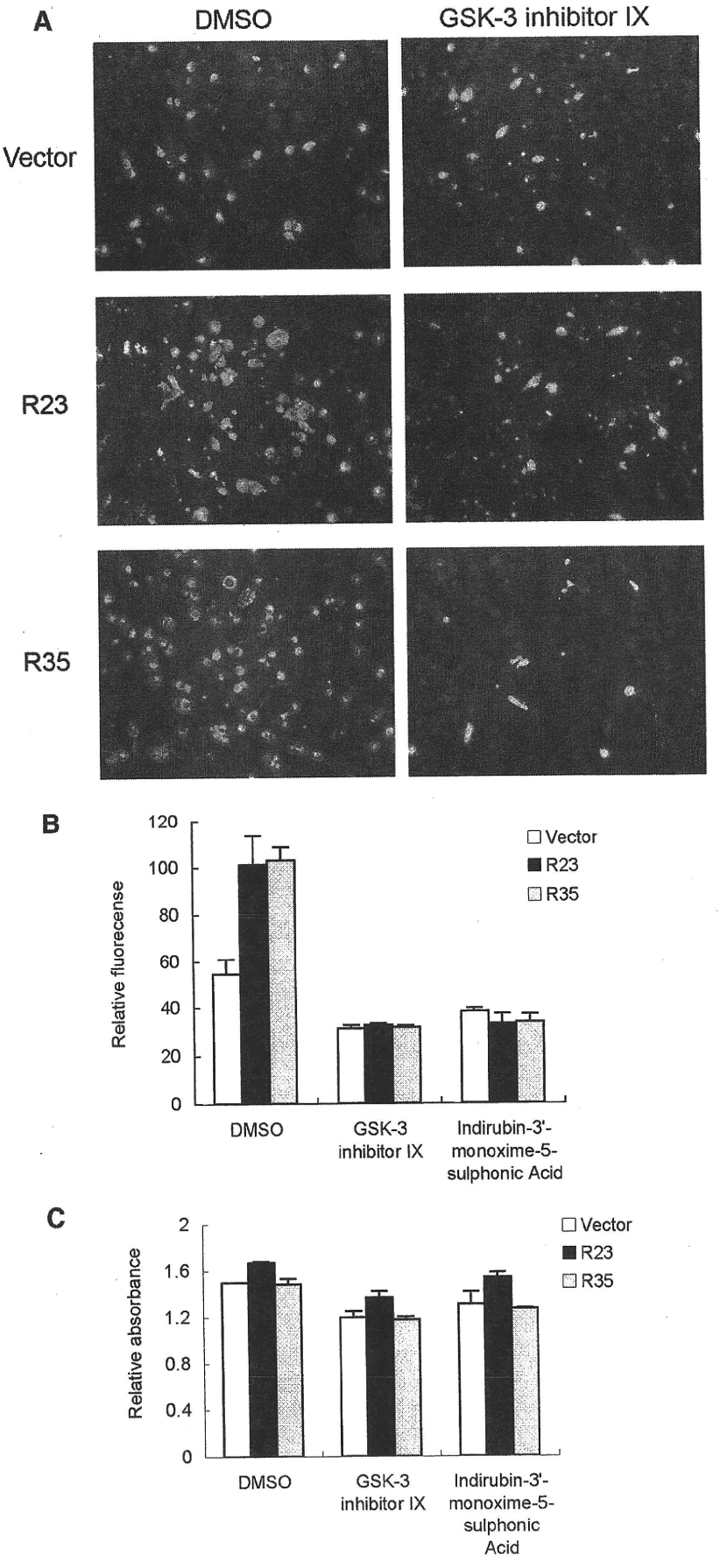
A
DMSO
GSK-3 inhibitor IX
Vector
R23
R35
B
Relative fluorecense
120
100
80
60
40
20
0
Vector
R23
R35
DMSO
GSK-3 inhibitor IX
Indirubin-3'-monoxime-5-sulphonic Acid
C
Relative absorbance
2
1.6
1.2
0.8
0.4
0
Vector
R23
R35
DMSO
GSK-3 inhibitor IX
Indirubin-3'-monoxime-5-sulphonic Acid

ble 1
al-time PCR analysis of human extracellular matrix and adhesion molecules.

Gene	Fold change
ADAM metallopeptidase with thrombospondin type 1 motif, 1	1.03
ADAM metallopeptidase with thrombospondin type 1 motif, 13	0.96
ADAM metallopeptidase with thrombospondin type 1 motif, 8	2.36
CD44 molecule	1.18
Cadherin 1, E-cadherin	0.68
Contactin 1	0.84
Collagen, type XI, alpha 1	1.03
Collagen, type XII, alpha 1	0.39
Collagen, type XIV, alpha 1	1.03
Collagen, type XV, alpha 1	1.45
Collagen, type XVI, alpha 1	1.03
Collagen, type I, alpha 1	1.03
Collagen, type IV, alpha 2	1.92
Collagen, type V, alpha 1	1.03
Collagen, type VI, alpha 1	0.63
Collagen, type VI, alpha 2	0.73
Collagen, type VII, alpha 1	1.03
Collagen, type VIII, alpha 1	1.03
Versican	1.03
Connective tissue growth factor	0.63
Catenin, alpha 1	0.78
Catenin, beta 1	0.84
Catenin, delta 1	0.9
Catenin, delta 2	1.03
Extracellular matrix protein 1	1.67
Fibronectin 1	1.36
Hyaluronan synthase 1	1.03
Intercellular adhesion molecule 1 (CD54)	0.73
Integrin, alpha 1	1.18
Integrin, alpha 2 (CD49B)	1.56
Integrin, alpha 3 (antigen CD49C)	1.27
Integrin, alpha 4 (antigen CD49D)	1.03
Integrin, alpha 5 (fibronectin receptor)	0.73
Integrin, alpha 6	0.96
Integrin, alpha 7	1.03
Integrin, alpha 8	1.03
Integrin, alpha L (antigen CD11A)	1.03
Integrin, alpha M	1.03
Integrin, alpha V (vitronectin receptor)	1.1
Integrin, beta 1 (fibronectin receptor)	0.84
Integrin, beta 2	0.84
Integrin, beta 3 (antigen CD61)	1.03
Integrin, beta 4	1.67
Integrin, beta 5	1.03
Kallmann syndrome 1 sequence	1.03
Laminin, alpha 1	1.1
Laminin, alpha 2 (merosin)	1.03
Laminin, alpha 3	1.03
Laminin, beta 1	1.27
Laminin, beta 3	0.9
Laminin, gamma 1	0.78
Matrix metallopeptidase 1	5.06
Matrix metallopeptidase 10 (stromelysin 2)	1.03
Matrix metallopeptidase 11 (stromelysin 3)	0.78
Matrix metallopeptidase 12	1.03
Matrix metallopeptidase 13 (collagenase 3)	1.03
Matrix metallopeptidase 14	1.79
Matrix metallopeptidase 15	0.59
Matrix metallopeptidase 16	1.03
Matrix metallopeptidase 2	1.03
Matrix metallopeptidase 3 (stromelysin 1)	1.03
Matrix metallopeptidase 7 (matrilysin)	1.03
Matrix metallopeptidase 8	1.03
Matrix metallopeptidase 9	0.9
Neural cell adhesion molecule 1	1.03
Platelet/endothelial cell adhesion molecule (CD31 antigen)	1.03
Selectin E	1.03
Selectin L	0.84
Selectin P (antigen CD62)	1.03
Sarcoglycan, epsilon	0.84
Osteonectin	1.03
Spastic paraplegia 7	1.18
Secreted phosphoprotein 1 (osteopontin)	1.03
Transforming growth factor-beta	1.1
Thrombospondin 1	1.18
Thrombospondin 2	1.03
Thrombospondin 3	0.9
TIMP metallopeptidase inhibitor 1	1.67
TIMP metallopeptidase inhibitor 2	0.96
TIMP metallopeptidase inhibitor 3	1.03
C-type lectin domain family 3, member B	1.03
Tenascin C	1.79
Vascular cell adhesion molecule 1	1.03
Vitronectin	0.55
Beta-2-microglobulin	1.45
Hypoxanthine phosphoribosyltransferase 1	1.1

Fold changes of R35 to Vector clone were calculated according to the instructions of the RT^{2}Profiler PCR Array.

Because our data indicate that the GSK-3 inhibitors tested abrogated prostate cancer cell migration to the basal level, GSK-3 is postulated to play a pivotal role in cell motility under the RhoB-involved signal cascade. The role of RhoB in GSK-3 signaling has already been demonstrated under hypoxic conditions (Skuli et al., 2006). Hypoxic signals induced RhoB-dependent Akt and GSK-3 phosphorylation. An RhoB-overexpressed R35 cell line did not show predominantly phosphorylated Akt (Thr308 and Ser473, data not shown); thus, signal transduction to GSK-3 might bypass Akt activation in this cell line.

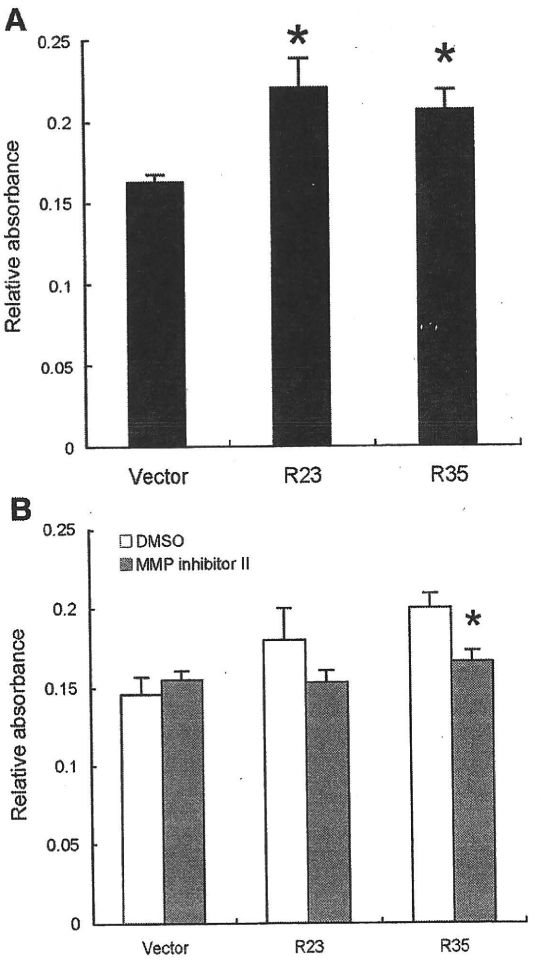

Fig. 3. Collagen gel invasion assays with or without MMP inhibitor. (A) Invasive potential of each clones were measured with Boyden chamber based assay system. Data shown are mean ± SD of triplicates, representation from three independent experiments. *$p<0.05$, compared to vector control. (B) Same collagen gel invasion assay in panel A, except each cells were pretreated with MMP inhibitor. Data shown are mean ± SD of triplicates, representation from three independent experiments. *$p<0.05$, compared to R35 DMSO. Mann–Whitney *U*-test was used to calculate statistical significances in panels A and B.

In addition to our current result, direct evidence showing that GSK-3 up-regulates epithelial cell migration has been presented using an MDCK wound closure assay (Farooqui et al., 2006). GSK-3 acts upstream of ADP-ribosylation factor 6 and Rac1, and the activated form of GSK-3 predominates during wound closure. The epithelial cell migration was blocked by an administration of GSK-3 inhibitor. The authors postulate that cell adhesion protein paxillin could be the downstream effecter molecule of GSK-3. Paxillin, which is a focal adhesion-associated protein, acts as a scaffold protein influencing cell motility and providing a signaling platform at the vicinity of focal adhesion (Brown and Turner, 2004). Since the phosphorylation of paxillin, which is essential in cell spreading, is mediated by GSK-3 and ERK dual-kinase (Cai et al., 2006), the phosphorylation levels of both proteins were evaluated in the R35 cell line. There was no difference in the phosphorylation status of GSK-3α (Ser21), GSK-3β (Ser9) and paxillin (Ser126) between R35 and vector cell lines (data not shown). GSK-3 phosphorylates target proteins preferably activated by other kinases (Doble and Woodgett, 2003). R35 and vector cells might have a different co-modifying set of kinases that target cell motile regulatory proteins.

Given the functional diversity, GSK-3 has been studied as a therapeutic target in many pathological conditions (Doble and Woodgett, 2003). Clinical and in vitro effects of GSK-3 inhibitors are insulin mimetic action, anti-cell proliferation and inhibition of tau phosphorylation. Recent studies have shown that administration of a GSK-3 inhibitor increased bone formation (Kulkarni et al., 2007) and prevented epithelial–mesenchymal transition (EMT) of human embryonic stem cell (Ullmann et al., 2008). EMT is the process of cytoskeletal and adhesion molecules to remodel an epithelial into mesenchymal phenotype, losing an original polarity but gaining a higher motility. Thus, close association of EMT with cancer invasion and metastasis, targeting GSK-3 by specific inhibitor, like our study and others, could become a therapeutic options for an advanced cancer.

The underlying mechanism between RhoB and MMP1 expression has not yet been fully elucidated. The cytoplasmic tail of a transmembrane mucin, MUC1, translocates to the nucleus after phosphorylation by Met, interacts with p53 and leads to the suppression of MMP1 transcription (Singh et al., 2008). MUC1 is also phosphorylated by GSK-3β (Li et al., 1998). The phosphorylation sites of MUC1 by Met and GSK-3β are not identical. So it is plausible that MUC1 in RhoB-overexpressed prostate cancer cells might be predominantly phosphorylated by GSK-3β, abrogating its suppressive effect on MMP1 transcription.

In the literature, there have been no solid data studying the relevance of RhoB and clinical cancer. One can assume that no correlation has been observed between clinical cancer and RhoB expression level. We did the compared real-time PCR experiment of RhoB in the cancer versus non-cancerous tissue from clinically dissected prostate cancer. The RhoB expression ratio (cancer/non-cancer) was diverse among each cancer cases and no correlation was observed toward Gleason score, an indicator of malignant potency and prognosis (data not shown). Based on the origin of DU145 cell line, which was derived from brain metastasis lesion, RhoB function as an invasion promoter might be exerted at distant metastatic prostate cancer. Even in this scenario, DNA demethylated and/or chromatin acetylated modification could be required for an induction of RhoB protein in prostate cancer cells as in our preliminary experiment.

In conclusion, this study presents the first evidence that RhoB promotes cellular motility and invasion of prostate cancer cell, signaling downstream in GSK-3 and enhancing a collagen gel invasion by MMP1 induction. Current results indicate that in certain cell type, like prostate cancer, RhoB works as a tumor promoter not as a suppressor. Unraveling the cell-type-specific bifunctional mechanisms and conditions of RhoB protein should help understanding the biological, physiological and pathological protein behavior.

References

Adamson, P., Paterson, H.F., Hall, A., 1992. Intracellular localization of the P21rho proteins. J. Cell Biol. 119, 617–627.

Allal, C., Pradines, A., Hamilton, A.D., Sebti, S.M., Favre, G., 2002. Farnesylated RhoB prevents cell cycle arrest and actin cytoskeleton disruption caused by the geranylgeranyltransferase I inhibitor GGTI-298. Cell Cycle 1, 430–437.

Brown, M.C., Turner, C.E., 2004. Paxillin adapting to change. Physiol. Rev. 84, 1315–1339.

Cai, X., Li, M., Vrana, J., Schaller, M.D., 2006. Glycogen synthase kinase 3- and extracellular signal-regulated kinase-dependent phosphorylation of paxillin regulates cytoskeletal rearrangement. Mol. Cell Biol. 26, 2857–2868.

Chen, Z., Sun, J., Pradines, A., Favre, G., Adnane, J., Sebti, S.M., 2000. Both farnesylated and geranylgeranylated RhoB inhibit malignant transformation and suppress human tumor growth in nude mice. J. Biol. Chem. 275, 17974–17978.

Doble, B.W., Woodgett, J.R., 2003. GSK-3: tricks of the trade for a multi-tasking kinase. J. Cell Sci. 116 (Part 7), 1175–1186.

Farooqui, R., Zhu, S., Fenteany, G., 2006. Glycogen synthase kinase-3 acts upstream of ADP-ribosylation factor 6 and Rac1 to regulate epithelial cell migration. Exp. Cell Res. 312, 1514–1525.

Jiang, K., Sun, J., Cheng, J., Djeu, J.Y., Wei, S., Sebti, S., 2004. Akt mediates Ras downregulation of RhoB, a suppressor of transformation, invasion, and metastasis. Mol. Cell. Biol. 24, 5565–5576.

Kozma, R., Ahmed, S., Best, A., Lim, L., 1995. The Ras-related protein Cdc42Hs and bradykinin promote formation of peripheral actin microspikes and filopodia in Swiss 3T3 fibroblasts. Mol. Cell. Biol. 15, 1942–1952.

Kulkarni, N.H., Wei, T., Kumar, A., Dow, E.R., Stewart, T.R., Shou, J., N'cho, M., Sterchi, D.L., Gitter, B.D., Higgs, R.E., Halladay, D.L., Engler, T.A., Martin, T.J., Bryant, H.U., Ma, Y.L., Onyia, J.E., 2007. Changes in osteoblast, chondrocyte, and adipocyte lineages mediate the bone anabolic actions of PTH and small molecule GSK-3 inhibitor. J. Cell Biochem. 102, 1504–1518.

Li, Y., Bharti, A., Chen, D., Gong, J., Kufe, D., 1998. Interaction of glycogen synthase kinase 3beta with the DF3/MUC1 carcinoma-associated antigen and beta-catenin. Mol. Cell. Biol. 18, 7216–7224.

Liu, A., Du, W., Liu, J.P., Jessell, T.M., Prendergast, G.C., 2000. RhoB alteration is necessary for apoptotic and antineoplastic responses to farnesyltransferase inhibitors. Mol. Cell. Biol. 20, 6105–6113.

Liu, A.X., Rane, N., Liu, J.P., Prendergast, G.C., 2001. RhoB is dispensable for mouse development but it modifies susceptibility to tumor formation as well as cell adhesion and growth factor signaling in transformed cells. Mol. Cell. Biol. 20, 6906–6912.

Moasser, M.M., Sepp-Lorenzino, L., Kohl, N.E., Oliff, A., Balog, A., Su, D.S., Danishefsky, S.J., Rosen, N., 1998. Farnesyl transferase inhibitors cause enhanced mitotic sensitivity to taxol and epothilones. Proc. Natl. Acad. Sci. U. S. A. 95, 1369–1374.

Murray, G.I., Duncan, M.E., O'Neil, P., Melvin, W.T., Fothergill, J.E., 1996. Matrix metalloproteinase-1 is associated with poor prognosis in colorectal cancer. Nat. Med. 2, 461–462.

Prendergast, G.C., 2001. Actin' up RhoB in cancer and apoptosis. Nat. Rev. Cancer 1, 162–168.

Ridley, A.J., Hall, A., 1992. The small GTP-binding protein rho regulates the assembly of focal adhesions and actin stress fibers in response to growth factors. Cell 70, 389–399.

Ridley, A.J., Paterson, H.F., Johnston, C.L., Diekmann, D., Hall, A., 1992. The small GTP-binding protein rac regulates growth factor-induced membrane ruffling. Cell 70, 401–410.

Sandilands, E., Cans, C., Fincham, V.J., Brunton, V.G., Mellor, H., Prendergast, G.C., Norman, J.C., Superti-Furga, G., Frame, M.C., 2004. RhoB and actin polymerization coordinate Src activation with endosome-mediated delivery to the membrane. Dev. Cell 7, 855–869.

Sauter, W., Rosenberger, A., Beckmann, L., Kropp, S., Mittelstrass, K., Timofeeva, M., Wölke, G., Steinwachs, A., Scheiner, D., Meese, E., Sybrecht, G., Kronenberg, F., Dienemann, H., Chang-Claude, J, Illig, T., Wichmann, H.E., Bickeböller, H., Risch, A., LUCY-Consortium, 2008. Matrix metalloproteinase 1 (MMP1) is associated with early-onset lung cancer. Cancer Epidemiol. Biomarkers Prev. 17, 1127–1135.

Schütz, A., Schneidenbach, D., Aust, G., Tannapfel, A., Steinert, M., Wittekind, C., 2002. Differential expression and activity status of MMP-1, MMP-2 and MMP-9 in tumor and stromal cells of squamous cell carcinomas of the lung,. Tumour. Biol. 23, 179–184.

Singh, P.K., Behrens, M.E., Eggers, J.P., Cerny, R.L., Bailey, J.M., Shanmugam, K., Gendler, S.J., Bennett, E.P., Hollingsworth, M.A., 2008. Phosphorylation of MUC1 by Met modulates interaction with p53 and MMP1 expression. J. Biol. Chem. 283, 26985–26995.

Skuli, N., Monferran, S., Delmas, C., Lajoie-Mazenc, I., Favre, G., Toulas, C., Cohen-Jonathan-Moyal, E., 2006. Activation of RhoB by hypoxia controls hypoxia-inducible factor-1alpha stabilization through glycogen synthase kinase-3 in U87 glioblastoma cells. Cancer Res. 66, 482–489.

Sternlicht, M.D., Werb, Z., 2001. How matrix metalloproteinases regulate cell behavior. Annu. Rev. Cell Dev. Biol. 17, 463–516.

Ullmann, U., Gilles, C., De Rycke, M., Van de Velde, H., Sermon, K., Liebaers, I., 2008. GSK-3-specific inhibitor-supplemented hESC medium prevents the epithelial–mesenchymal transition process and the up-regulation of matrix metalloproteinases in hESCs cultured in feeder-free conditions. Mol. Hum. Reprod. 14, 169–179.

Wheeler, A.P., Ridley, A.J., 2004. Why three Rho proteins? RhoA, RhoB, RhoC, and cell motility. Exp. Cell Res. 301, 43–49.

Wheeler, A.P., Ridley, A.J., 2007. RhoB affects macrophage adhesion, integrin expression and migration. Exp. Cell Res. 313, 3505–3516.

Wherlock, M., Gampel, A., Futter, C., Mellor, H., 2004. Farnesyltransferase inhibitors disrupt EGF receptor traffic through modulation of the RhoB GTPase. J. Cell Sci. 117 (Part 15), 3221–3231.

Inhalation Toxicology, 2009; 21(11): 898–905

informa
healthcare

RESEARCH ARTICLE

Effect of polymerized toner on rat lung in chronic inhalation study

Yasuo Morimoto[1], Masami Hirohashi[1], Takahiko Kasai[2], Takako Oyabu[1], Akira Ogami[1], Toshihiko Myojo[1], Masahiro Murakami[1], Ken-ichiro Nishi[1], Chikara Kadoya[1], Motoi Todoroki[1], Makoto Yamamoto[1], Kazuaki Kawai[1], Hiroshi Kasai[1], and Isamu Tanaka[1]

[1]*Department of Occupational Pneumology, Institute of Industrial Ecological Sciences, University of Occupational and Environmental Health, Japan, Kitakyushu, Japan, and* [2]*Department of Diagnostic Pathology, Nara Medical University, Nara, Japan*

Abstract

In order to evaluate the chronic effect of polymerized toner particles on the lung, inflammation- and fibrosis-related genes were analyzed and 8-hydroxydeoxyguanosine (8-OHdG) was examined by using the lung tissue of rats subjected to 24 months of toner inhalation exposure. Wistar female rats were divided into four groups (5 weeks old, 30 rats in each): the high concentration exposure group (16.3 ± 0.6 mg/m³), the medium concentration exposure group (4.4 ± 0.3 mg/m³), the low concentration exposure group (1.6 ± 0.2 mg/m³), and the control group (clean air). The material used was black toner, and its aerodynamic diameter in the exposure chamber was 3.0 μm. The rats were exposed to the material for 24 months (6 hours/day, 5 days/week) and dissected after the exposure period. RNA was extracted from one lung and the gene expression related to inflammation and fibrosis. Matrix metalloproteinase-2 (MMP-2), tissue inhibitor of metalloproteinase-2 (TIMP-2), and type I collagen were analyzed according to the ratio of each gene/β-actin. Also, 8-OHdG level in the lung tissue was measured by HPLC with an electrochemical detector. Small fibrotic foci were found in the toner exposed groups; however, progressive or irreversible fibrosis was not found. The incidence of small fibrotic foci and cell aggregation increased in a dose-dependent manner. There were no significant differences of expression of MMP-2, TIMP-2, and type I collagen between the control group and each exposed group. Lung tumors did not develop in each group. A significant production of 8-OHdG was not observed in the toner exposed groups. In conclusion, toner produced by polymerization was not associated with evidence of carcinogenesis in this experiment.

Keywords: *Polymerised toner; inhalation; rat; lung; fibrosis*

Introduction

Since toner for copiers and printers is widely used in many countries, occupational exposure may occur not only in production facilities but also in offices. Case reports on pneumoconiosis and hypersensitivity pneumonitis caused by toner have been published (Armbruster et al., 1996; Gallardo et al., 1994), and recently, fine particle generation by printers and allergy symptoms in printer users have been reported (Crijins et al., 1987). Thus, the biological effect of toner has become a concern. However, the causal relationship between toner and its effect on health is unknown.

There have been developments within toner manufacturing, and in addition to the conventional grinding process, the polymerization process has recently been used more widely, and its demand is increasing (Nanya et al., 2004). Differences in the toner manufacturing process may lead to differences in physicochemical properties of toner particles, thereby bringing about different biological effects. It is reported that the toner particle produced by polymerization has a smaller diameter, a narrower size range, and a smoother surface than those of the toner particle produced by grinding. Studies have reported that a finer particle size enhances biological response (Oberdorster et al., 2005) and toner surface properties influence its surface activity; thus, the biological effect is assumed to be different between ground and polymerized particles.

Pulmonary fibrosis and cancer are major pathologies caused by a chronic effect of particle exposure, and are typical pathological endpoints for hazard evaluation (Morimoto et al., 2005a, 2005b). In fibrosis, a major prerequisite lesion

Address for Correspondence: Yasuo Morimoto, Department of Occupational Pneumology, Institute of Industrial Ecological Sciences, University of Occupational and Environmental Health, Japan, 1-1 Iseigaoka Yahatanishiku, Kitakyushu, Japan. E-mail: yasuom@med.uoeh.ac.jp

(Received 27 August 2008; revised 17 November 2008; accepted 19 November 2008)

ISSN 0895-8378 print/ISSN 1091-7691 online © 2009 Informa UK Ltd
DOI: 10.1080/08958370802641938

is an excess deposition of matrix, i.e. collagen, in association with an imbalance between the production and degradation systems of collagen (Seyer et al., 1976; Woessner, 1991), and the increased imbalance is assumed to lead to fibrosis. Matrix metalloproteinases (MMPs) for collagen production are associated with the former, and the balance between MMPs for collagen metabolism and tissue inhibitors of metalloproteinase (TIMPs) to suppress collagen metabolism is associated with the latter. In regard to cancer, DNA damage caused by oxidative stress may result in gene mutation and eventually in carcinogenesis. Studies have reported that a marker of typical oxidative damage of DNA, 8-hydroxydeoxyguanosine (8-OHdG), is associated with carcinogenesis of various organs including the lung, and is a biomarker of lung cancer (Farinati et al., 1998; Kasai & Nishimura, 1984).

In order to evaluate the biological effect of polymerized toner, we examined the matrix system and production of 8-OHdG in the lung tissue of rats exposed to air containing polymerized toner for 24 months.

Materials and methods

Materials

The polymerized toner used in the present study was Imagio Toner Type 26 Black (Ricoh Company, Ltd.). The composition of this toner is >80% polyester resin, 1–10% wax, 1–10% silica, and 1–10% carbon black, as listed by the manufacturer. Scanning electron micrographs of toner particles in an exposure chamber are shown in Figure 1. The particle size distribution was determined by an Andersen cascade impactor (AN-200; Sibata Sci. Tech. Co., Japan). The mass median aerodynamic diameter and geometric standard deviation were 3.0 ± 1.7 μm.

Inhalation system (Figure 2)

The inhalation system consisted of a dust generator, exposure chambers (volume 0.57 m^3), and gas–liquid–solid separators, as described by Tanaka et al. (1983). A continuous fluidized bed was used as the dust generator. Toner was fed from the dust generator into the exposure chamber with the feed rate being controlled by the rotating speed of the screw feeder and the flow rate for fluidization. The toner aerosol concentration in the exposure chamber was measured daily by the isokinetic suction of air though a glass fiber filter beside the chamber. The glass fiber filter was weighed before and after the measurements in accordance with the standard method in JIS-Z8808, and the measured daily exposure weight concentration was determined as mg/m^3.

During exposure rats were kept in this chamber, and it was cleaned at the end of each exposure day. The rats were fed pellet-type food, and their weight was measured once a week.

Animals

One hundred twenty specific pathogen-free female Wistar rats, 5 weeks of age, were purchased from Kyudo (Kumamoto, Japan). These rats were divided into four groups: high exposure, medium exposure, low exposure, and a control group. Each group totaled 30 rats, which were then divided into 10 and 20 rats for the 12 and 24 months inhalation groups, respectively. The exposure groups were subjected to inhalation exposure for 6 hours a day, 5 days a week for up to 2 years (Tanaka et al., 1983). Daily average exposure concentrations and standard deviations in the low, medium, and high exposure groups were 1.6 + 0.2, 4.4 + 0.3, and 16.3 + 0.6 mg/m^3, respectively. The control rats were exposed to only clean air in a same-sized chamber located in the same air-conditioned room.

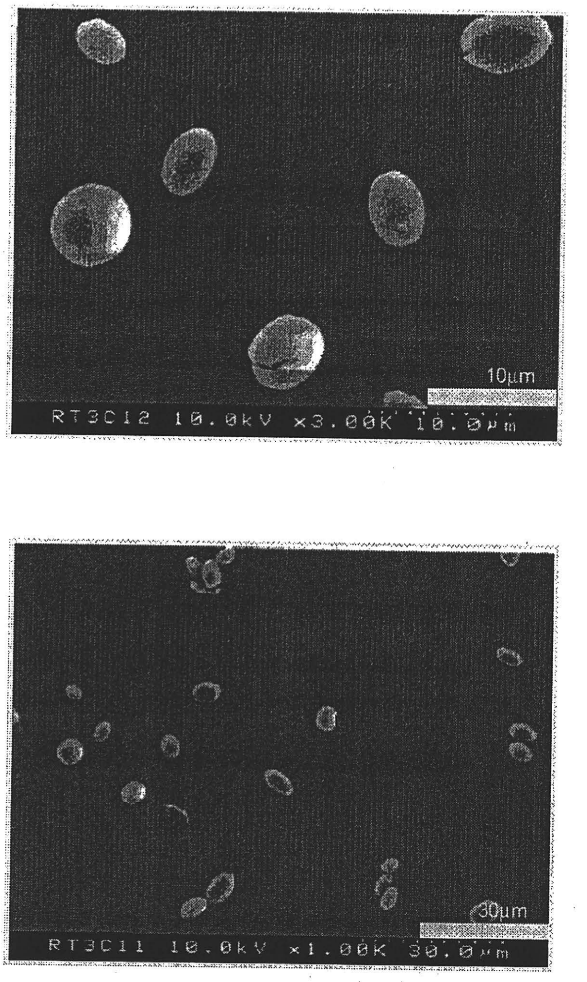

Figure 1. Scanning electron micrographs of toner particles in exposure chamber.

After 1 or 2 years of inhalation exposure, the rats were injected intraperitoneally with a fatal overdose of phenobarbital. The rats were handled according to the guidelines described in the Japanese *Guide for the care and use of laboratory animals* as approved by the Animal Care and Use Committee, University of Occupational and Environmental Health, Japan.

Periodic tests for microorganisms such as viruses, bacteria, and mycoplasma were carried out using sentinel rats

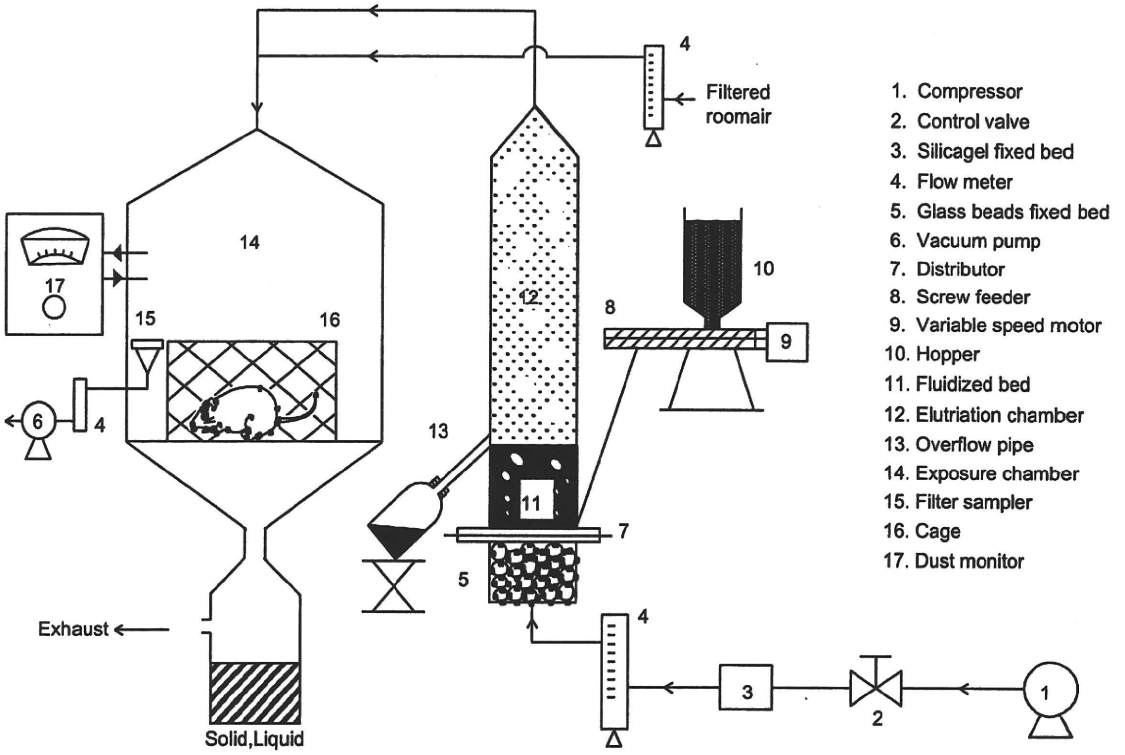

Figure 2. Schematic diagram of dust exposure system.

during the experiment, and pathogens were not observed in the rats.

Preparation of RNA, cDNA synthesis, and polymerase chain reaction

Total RNA from the lung was prepared in the presence of guanidium thiocyanate (Chomczynski & Sacchi, 1987). Single-strand cDNA was synthesized with Moloney murine leukemia virus-derived reverse transcriptase (Perkin Elmer, Norwalk, CT) using 500 ng of total RNA. An equal amount of cDNA from each sample was amplified by specific primers for each gene. Amplification was performed with a thermocycler (Astech, Japan) under the following conditions: denaturation at 94°C for 45 seconds, annealing at 60°C for 45 seconds, and extension at 72°C for 2 minutes for the target and β-actin genes.

The fragments amplified by polymerase chain reaction (PCR) were detected by electrophoresis on 2% agarose gel. The PCR products were resolved using gel electrophoresis and visualized by ethidium bromide staining. The gel was photographed with Polaroid type 665 positive/negative film (Polaroid Corp., Cambridge, MA) under ultraviolet light at identical exposure and development times. The bands from the positive film were scanned, and the density of MMP-2, TIMP-2, and type I collagen PCR product was measured using National Institute of Health (NIH) Image 1.55 software (written by Wane Rasband at NIH, Bethesda, MD).

Analysis of 8-OHdG in lung DNA

The 8-OHdG level in the DNA of lungs exposed to the toner was measured according to previously described methods (Kawai et al., 2007). Briefly, cellular DNA from rat lungs (n = 8) was isolated using a DNA extractor WB Kit (Wako, Japan). The isolated DNA was digested with nuclease P1 (Yamasa, Japan) and alkaline phosphatase to obtain 8-OHdG in the nucleoside form. The nucleoside solution was filtered with Ultrafree-Probind (Millipore, Billerica, MA) and was injected into a high-performance liquid chromatography (HPLC) column (Shiseido Capcell Pak C18 MG 4.6 × 250 mm; Tokyo, Japan) equipped with an electrochemical detector (ECD-300; Eicom Co., Kyoto, Japan) with a flow rate of 1.0 ml/min. The mobile phase consisted of 10 mM NaH_2PO_4 containing 8% methanol. 8-OHdG in DNA was calculated as 8-OHdG/10^6 dG.

Statistical analysis

Statistical analysis was carried out using the Mann–Whitney test with differences at $p < 0.05$ considered to be statistically significant.

Tissue preparation for H&E stain

After removal of the lungs, the left lung was inflated and fixed by intratracheal instillation of 4% paraformaldehyde at 25 cm H_2O pressure. The lungs and trachea were resected from the surrounding tissue, and allowed to stand at 4°C for 24 hours. The tissue was washed for 10 minutes

in phosphate-buffered saline, dehydrated by immersion in a graded series of ethanol washes for 1 hour per wash, then maintained in 100% ethanol at 4°C. The lung tissue was embedded in paraffin, and 5 μm-thick sections were cut from the lobe. The samples were then sectioned and stained with hematoxylin and eosin (H&E). The lung pathology was scored 0–5 for fibrotic change, according to the methods described. ESP scores, criteria for fibrosis at the bronchiolar–alveolar junction, were as follows (Bernstein et al., 2006): grade 0, a normal lung; grade 1, minimal, just detectable, very few, very small foci of collagen deposition; grade 2, slight, fairly easily detected, few, small foci of collagen deposition; grade 3, moderate, easily detected foci of collagen deposition in considerably enlarged areas at the bronchiolar–alveolar junction; grade 4, marked, obvious, or extensive foci of collagen deposition extending from the bronchiolar–alveolar junction into the interstitium of more peripheral parts of the lung parenchyma; grade 5, severe, widespread collagen deposition with consolidation at the bronchiolar–alveolar junction, sometimes with interlobular linking. The severity of the fibrotic changes in each lung section was assessed as a mean score of severity from the observed fibrotic fields.

In order to quantify inflammation in H&E-stained lung specimens, the areas of inflammation were determined. Six random digital images were taken per lung section with a digital camera (DS-5M; Nikon Instech Co. Ltd., Kanagawa, Japan) under light microscopy. A 300-point grid was placed over each image on the computer screen and we examined pulmonary inflammation in each using the point counting method. The percentage area of inflammation, excluding air spaces in the lung parenchyma, was calculated (Ogami et al., 2009).

Results

Survival rate

The number of deaths at earlier than 24 months was eight in the control group, 10 in the low concentration exposure group, nine in the medium concentration exposure group, and six in the high concentration exposure group, and there was no difference of survival rate among the four groups. In addition, there was no difference of behavior.

Wet weight of organs

There were no differences in wet weights of the lungs, liver, kidneys, and spleen among the control group and the exposed groups at 12 months and at 24 months.

Pathological findings of the lung

The pathological findings of the lung are shown in Table 1 (at 12 months), Table 2 (at 24 months), and Figure 3.

No tumors, including benign tumors, were found in the exposed group at 12 and 24 months. There was no dysplasia of alveolar and respiratory epithelia in the exposed groups, although hyperplasia was observed in all groups.

Small fibrotic foci and cell aggregation were not found in the control group after 12 months; however, small fibrotic foci, i.e. mild fibrosis, was found in the toner exposed groups. After 24 months, small fibrotic foci or mild fibrosis was observed in the toner exposed groups, and the morbidity of small fibrotic foci was higher in the high concentration exposure group. However, the ESP score showed local mild fibrosis of level 1 or 2, and inhaled toner was localized around cell aggregation in alveoli. Progressive or irreversible fibrosis, which is observed in the case of exposure to crystalline silica and asbestos, was not observed.

We also quantified inflammation in lungs according to the inflammation area (Figure 4). Compared to controls, no significant increase in inflammation score was observed in the exposed groups at either 12 or 24 months.

Type I collagen gene expression

There was no significant difference in gene expression of β-actin between the control and toner-exposed groups. Figure 5 shows type I collagen expression after 12 and 24 months. There was no significant difference of expression between the control group and each exposed group after 12 months. Similarly, no significant difference of expression was

Table 1. Pathological findings in rat lungs at 1 year of toner inhalation.

	Small foci of collagen (n (%))	Accumulation of macrophages (n (%))	Bronchial pneumonia (n (%))	Tumors (n (%))	Pleural thickening (n (%))
Control (n = 10)	0 (0)	0 (0)	0 (0)	0 (0)	0 (0)
Low concentration exposure group (n = 10)	2 (20)	3 (30)	0 (0)	0 (0)	0 (0)
Medium concentration exposure group (n = 10)	2 (20)	3 (30)	0 (0)	0 (0)	0 (0)
High concentration exposure group (n = 10)	5 (50)	3 (30)	2 (20)	0 (0)	0 (0)

Table 2. Pathological findings in rat lungs at 2 years of toner inhalation.

	Small foci of collagen (n (%))	Accumulation of macrophages (n (%))	Bronchial pneumonia (n (%))	Tumors (n (%))	Pleural thickening (n (%))
Control (n = 12)	2 (17)	4 (33)	2 (17)	1 (8)	0 (0)
Low concentration exposure group (n = 10)	3 (30)	1 (10)	1 (10)	0 (0)	0 (0)
Medium concentration exposure group (n = 11)	3 (27)	2 (18)	0 (0)	0 (0)	0 (0)
High concentration exposure group (n = 14)	9 (64)	7 (50)	1 (7)	0 (0)	0 (0)

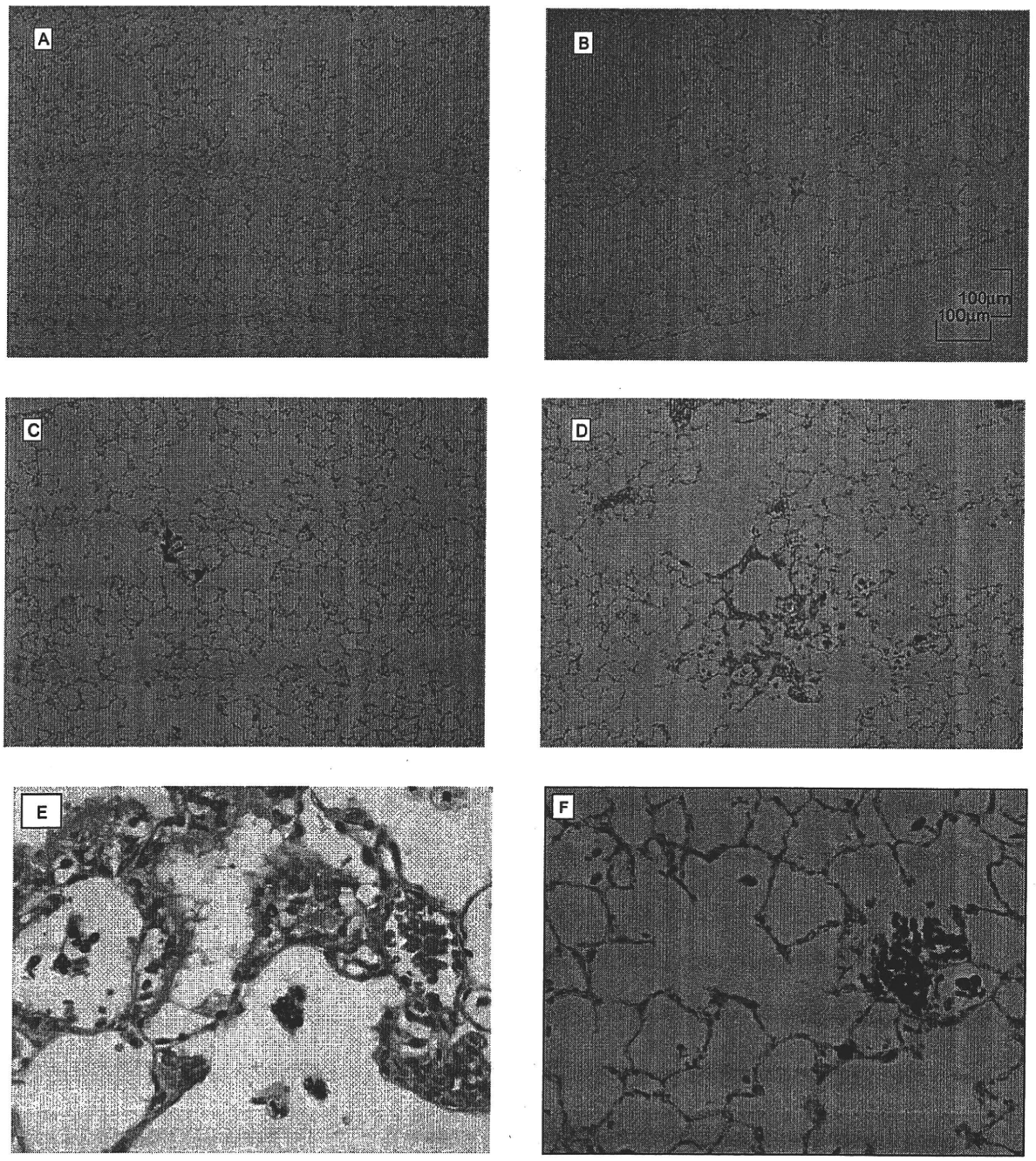

Figure 3. Pathological findings in lung tissue: small fibrotic foci. (A) Control group; (B) low exposure group; (C) medium exposure group; (D) high exposure group; (E) aggregates of alveolar macrophages and alveolar epithelial hyperplasia in high exposure group, ×400; (F) aggregates of alveolar macrophages with inhaled toner in alveoli in high exposure group, ×400.

found between the control group and each exposed group after 24 months.

TIMP-2 gene expression

TIMP-2 gene expression after 12 and 24 months is shown in Figure 6. There was no significant difference of expression in the low, medium, and high concentration exposure groups as compared with the control group after both 12 and 24 months.

MMP-2 gene expression

MMP-2 gene expression after 12 and 24 months is shown in Figure 7. No significant difference of expression was found between the control and each exposed group after 12 months.

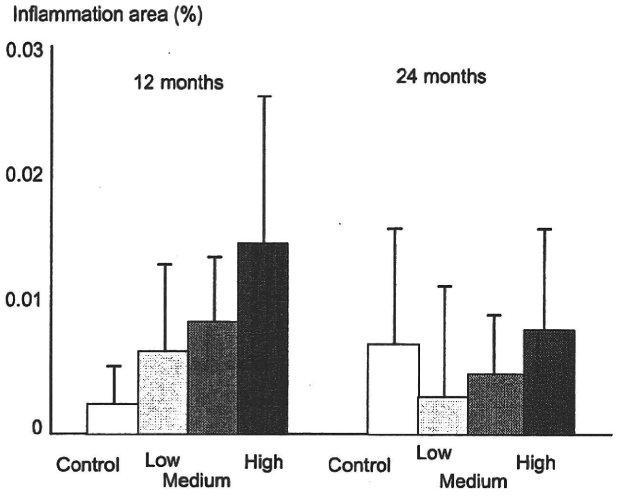

Figure 4. Inflammation area of lung tissue according to point counting methods, control and low, medium, and high exposure groups. Error bar: standard deviation.

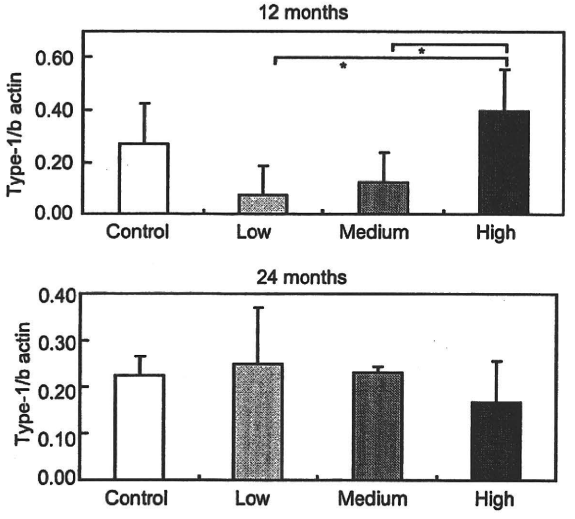

Figure 5. Gene expression of type I collagen in rat lungs, control and low, medium, and high exposure groups. Error bar: standard deviation. *$p < 0.05$ compared with control group.

After 24 months, increased expression was observed in the medium concentration exposure group; however, this increase was not a consistent change. There was no significant difference between the control group and each exposed group.

Formation of 8-OHdG

Formation of 8-OHdG after 12 and 24 months is shown in Figure 8. As compared to the control group, there was no significant production in each exposed group after 12 and 24 months.

Discussion

Inhalation exposure to polymerized toner for 24 months caused mild and local fibrosis in rat lung in a dose-dependent

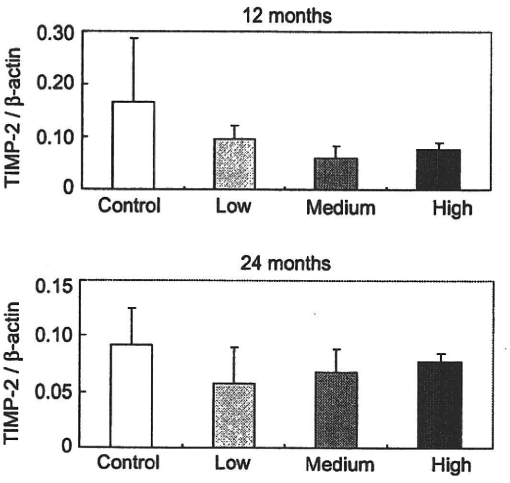

Figure 6. Gene expression of TIMP-2 in rat lungs, control and low, medium, and high exposure groups. Error bar: standard deviation.

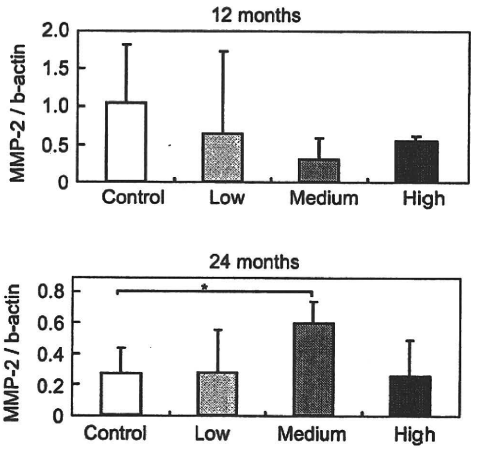

Figure 7. Gene expression of MMP-2 in rat lungs, control and low, medium, and high exposure groups. Error bar: standard deviation. *$p < 0.05$ compared with control group.

manner. The few previous studies (Bellmann et al., 1991, 1992; Muhle et al., 1991) carried out in the early 1990s indicated a relationship between the inhalation of toner and pulmonary fibrosis in animal models. Muhle et al. (1991) reported that a mild to moderate degree of lung fibrosis was observed in 2-year inhalation studies. These reports did not refer to the manufacturing process of the toner.

We previously conducted a 2-year inhalation exposure study using ground toner and found similar mild fibrosis (Morimoto et al., 2005a). On this basis, there was no marked difference of intrapulmonary response comparing toner manufacturing processes. However, the EPS score for ground toner was at level 2–3, while that for polymerized toner was at level 1–2. As compared with ground toner, polymerized toner has a smaller, relatively uniform diameter. Thus it is supposed that its surface area and particle count per unit weight are increased, though the particle surface is smooth.

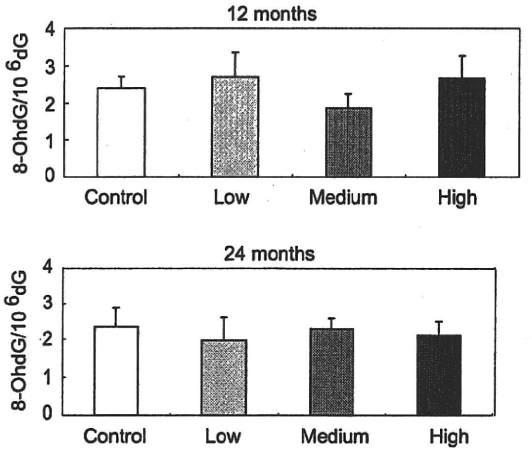

Figure 8. Formation of 8-hydroxydeoxyguanosine (8-OHdG) in rat lungs, control and low, medium, and high exposure groups. Error bar: standard deviation

The former properties will accelerate the response, while the latter property will suppress the response. In light of the EPS results in the present study, the effect of the latter property might be reflected.

Besides, the polymerized toner did not induce any significant changes of gene expression of MMP, TIMP, and collagen after 12 and 24 months. In our previous study using ground toner, the expression of collagen and MMP was elevated after 12 months, and TIMP and collagen increased after 24 months (Morimoto et al., 2005a); these changes of gene expression were suggested to be associated with mild fibrosis. Since these gene expressions were not observed in the present study, it is suggested that matrix production- and metabolism-related genes are little involved in very mild fibrosis.

Pathological findings revealed local toner retention only around cell aggregates in alveoli. A small amount of toner may be retained in rat lung, based on the pathological findings. Moreover, because active fibrotic lesions such as fibroblast foci were not observed, it is suggested that fibrosis was minor. There were no new findings such as plaque near the visceral and parietal pleura; this is consistent with the previous study. Since inflammatory cell infiltration was little and there were no pleural lesions, it is suggested that a very small amount of toner was transferred to around the pleura by lymph.

Long-term inhalation exposure to polymerized toner did not induce significant carcinogenesis in the lung. Neither tumor nor fibrosis was found in lung tissue in intratracheal instillation experiments using micron size carbon black, the main component of toner (Nau et al., 1960; Sano, 1959). Also, Muhle et al. (1991) reported no increase of carcinogenesis in an inhalation exposure study using hamsters for 18 months to examine chronic effects, although fibrosis was observed. Mohr et al. (2006) intratracheally injected a high dose of toner (60–120 mg) into rats and induced lung tumors. One cause of these differences in tumor morbidity may be different deposition amounts in the lung. Studies reported that insoluble, low toxicity particles such as titanium dioxide and carbon black resulted in low carcinogenicity up to a certain exposure level; however, when the exposure level exceeded a threshold, their carcinogenicity increased rapidly. This suggests that excessive administration induces carcinogenicity (ILSI Risk Science Institute Workshop Participants, 2000). Our previous long-term inhalation exposure study using ground toner showed a lung deposition of 0.22–1 mg (Oyabu et al., 2001). The diameter of the toner particle in the present study was smaller; however, the exposure level was nearly the same, and thus the lung deposition is assumed to be in the same range. Bellmann et al. (1991) examined lung deposition in an inhalation study in rats at 0.22–16 mg/m^3, and reported delayed clearance at 16 mg/m^3. This concentration was the same level as our high concentration exposure level in the present study, so the exposure level in the present study is likely to be at this threshold or lower.

The formation of a marker of oxidative DNA damage, 8-OHdG, did not increase in lung tissue by exposure to polymerized toner. An in vitro study of 8-OHdG reported that when the alveolar epithelium cell line A549 was exposed to crocidolite, which is an asbestos with carcinogenicity, significant increases of 8-OHdG production and its repairing enzyme activity were observed (Kim et al., 2001) In J774 cells derived from macrophages, exposure to crocidolite and amosite caused significant formation of 8-OHdG (Murata-Kamiya et al., 1997). Xu et al. (1999) also exposed human-hamster hybrid cells to crocidolite and observed the formation of 8-OHdG, confirming that active oxygen species such as OH radicals are involved in DNA mutagenesis by asbestos in a dose-dependent manner in such responses. On the other hand, a low toxicity substance, glass fiber, classified in group 3 of the carcinogenic substance classification by the International Agency for Research on Cancer (IARC), did not cause significant formation of 8-OHdG in J774 cells (Murata-Kamiya et al., 1997). Yamaguchi et al. (1999) intratracheally injected crocidolite into rats and observed significant production, however. Intratracheal injection of ultra-fine colloidal silica resulted in the formation of 8-OHdG in alveolar epithelial cells and alveolar macrophages (Kaewamatawong et al., 2006). In another study, intratracheal injection of low toxicity glass fiber did not cause significant production (Yamaguchi et al., 1999). Moreover, in our 2-year inhalation exposure study using ground toner, no carcinogenesis or significant 8-hydroxydeoxyguanosine formation in the lung was observed (Morimoto et al., 2005b). As can be seen from the above, the formation of 8-OHdG both in vivo and in vitro is correlated to the carcinogenicity of chemicals. Therefore, in consideration of no 8-OHdG formation with polymerized toner, these results support that carcinogenesis by polymerized toner was not observed.

In conclusion, in an inhalation study of toner for 24 months using Wistar rats divided into three groups (high, middle, and low concentration exposure groups, 6 hours/day, 5 days/week), lung tumors were not found, while mild fibrosis was observed in a dose-dependent manner. Moreover, there were no significant changes of matrix-

related gene expression and 8-OHdG formation. In conclusion, toner produced by polymerization was not associated with evidence of carcinogenesis in this experiment.

Declaration of interest: The authors report no conflicts of interest. The authors alone are responsible for the writing of this paper.

References

Armbruster C, Dekan G, Hovorka A. 1996. Granulomatous pneumonitis and mediastinal lymphadenopathy due to photocopier toner dust. *Lancet* 348:690.

Bellmann B, Muhle H, Creutzenberg O, Dasenbrock C, Kilpper R, MacKenzie JC, Morrow P, Memelstein R. 1991. Lung clearance and retention of toner, utilizing a tracer technique, during chronic inhalation exposure in rats. *Fundam Appl Toxicol* 17:300–313.

Bellmann B, Muhle H, Creutzenberg O, Mermelstein R. 1992. Irreversible pulmonary changes induced in rat lung by dust overload. *Environ Health Perspect* 97:189–191.

Bernstein DB, Rogers R, Smith P, Chevalier J. 2006. The toxicological response of Brazilian chrysotile asbestos: A multidose subchronic 90-day inhalation toxicology study with 92-day recovery to assess cellular and pathological response. *Inhal Toxicol* 18:313–332.

Chomczynski P, Sacchi N. 1987. Single-step method of RNA isolation by acid guanidinium thiocyanate-pheno-chloroform extraction. *Anal Biochem* 162:156–159.

Crijns MB, Boom BW, van der Schroeff JG. 1987. Allergic contact dermatitis to a diazonium compound in copy paper. *Contact Dermatitis* 16:112–113.

Farinati F, Cardin R, Degan P, Rugge M, Mario FD, Bonvicini P, Naccarato R. 1998. Oxidative DNA damage accumulation in gastric carcinogenesis. *Gut* 42(3):351–356.

Gallardo M, Romero P, Sanchez-Quevedo MC, Lopez-Caballero JJ. 1994. Siderosilicosis due to photocopier toner dust. *Lancet* 344:412–413.

ILSI Risk Sceince Institute Workshop Participants. 2000. The relevance of the rat lung response to particle overload for human risk assessment: A workshop consensus report. *Inhal Toxicol* 12:1–17.

Kaewamatawong T, Shimada A, Okajima M, Inoue H, Morita T, Inoue K, Takano H. 2006. Acute and subacute pulmonary toxicity of low dose of ultrafine colloidal silica particles in mice after intratracheal instillation. *Toxicol Pathol* 34:958–965.

Kasai H, Nishimura S. 1984. Hydroxylation of deoxyguanosine at the C-8 position by ascorbic acid and other reducing agents. *Nucleic Acids Res* 12(4):2137–2145.

Kawai K, Li YS, Kasai H. 2007. Accurate measurement of 8-OH-dG and 8-OH-Gua in mouse DNA urine and serum: Effect of X-ray irradiation. *Genes Environ* 29:107–114.

Kim HN, Morimoto Y, Tsuda T, Ootsuyama Y, Hirohashi M, Hirano T, Tanaka I, Lim Y, Yun IG, Kasai H. 2001. Changes in DNA 8-hydroxyguanine levels, 8-hydroxyguanine repair activity, and hOGG1 and hMTH1 mRNA expression in human lung alveolar epithelial cells induced by crocidolite asbestos. *Carcinogenesis* 22(2):265–269.

Mohr U, Ernst H, Roller M, Pott F. 2006. Pulmonary tumor types induced in Wistar rats of the so-called "19-dust study". *Exp Toxicol Pathol* 58:13–20.

Morimoto Y, Kim H, Oyabu T, Hirohashi M, Nagatomo H, Ogami A, Yamato H, Higashi T, Tanaka I, Kasai T. 2005. Effect of long-term inhalation of toner on extracellular matrix in the lungs of rats in vivo. *Inhal Toxicol* 17:153–159.

MorimotoY, Kim H, Oyabu T, Hirohashi M, Nagatomo H, Ogami A, Yamato H, Obata Y, Kasai H, Higashi T, Tanaka I. 2005. Negative effect of long-term inhalation of toner on formation of 8-hydroxydeoxyguanosine in DNA in the lungs of rats in vivo. *Inhal Toxicol* 17:749–753.

Muhle H, Bellmann B, Creutzenberg O, Dasenbrock C, Ernst H, Kilpper R, et al. 1991. Pulmonary response to toner upon chronic inhalation exposure in rats. *Fundam Appl Toxicol* 17:280–299.

Murata-Kamiya N, Tsutsui T, Fujino A, Kasai H, Kaji H. 1997. Determination of carcinogenic potential of mineral fibers by 8-hydroxydeoxyguanosine as a marker of oxidative DNA damage in mammalian cells. *Int Arch Occup Environ Health* 70(5):321–326.

Nanya T, Sasaki F, Yagi S, Shimota N, Higuchi H, Awamura J, Tomita M. 2004. *Development of a new polyester-based polymerization toner.* In IS & T's NIP20: International Conference on Printing Technologies, pp. 143–147. Springfield, VA: The Society for Imaging Science and Technology.

Nau CA, Neal J, Stembridge VA. 1960. A study of the physiological effects of carbon black. Adsorption and elution potentials; Subcutaneous injections. *Arch Environ Health* 1:512–533.

Oberdorster G, Oberdorster, Oberdorster J. 2005. Nanotoxicology: An emerging discipline evolving from studies of ultrafine particles. *Environ Health Perspect* 113:823–839.

Ogami A, Morimoto Y, Myojo T, Oyabu T, Murakami M, Todoroki M, Nishi K, Kadoya C, Yamamoto M, Tanaka I. 2009. Pathological features of different sizes of nickel oxide following intratracheal instillation in rats. *Inhal Toxicol* in press.

Oyabu T, Yamato H, MorimotoY, Ogami A, Yamamura K, Tanaka I. 2001. Biopersistence of toner particles in rat lungs during 2 years inhalation. *J Aerosol Res* 16(S):94–95.

Sano T. 1959. Experiment studies on pneumoconiosis by dust contained 10% of silica. *Rodo Kagaku* 35:700 (in Japanese).

Seyer JM, Hutcheson ET, Kang AH. 1976. Collagen polymorphism in idiopathic chronic pulmonary fibrosis. *J Clin Invest* 57:1498–1507.

Tanaka I, Matsuno K, Kodama Y, Akiyama T. 1983. Pulmonary deposition of a fly ash aerosol by inhalation. *J UOEH* 5(4):423–431.

Woessner JF Jr. 1991. Matrix metalloproteinases and their inhibitors in connective tissue remodeling. *FASEB J* 5:2145–2154.

Xu A, Wu LJ, Santella RM, Hei TK. 1999. Role of oxyradicals in mutagenicity and DNA damage induced by crocidolite asbestos in mammalian cells. *Cancer Res* 59:5922–5926.

Yamaguchi R, Hiirano T, Ootsuyama Y, Asami S, Tsurudome Y, Fukada S, Yamato H, Tshuda T, Tanaka I, Kasai H. 1999. Increased 8-hydroxyguanine in DNA and its repair activity in hamster and rat lung after intratracheal instillation of crocidolite asbestos. *Jpn J Cancer Res* 90(5):505–509.

DNA Methylation at the C-5 Position of Cytosine by Methyl Radicals: A Possible Role for Epigenetic Change during Carcinogenesis by Environmental Agents

Hiroshi Kasai* and Kazuaki Kawai

Department of Environmental Oncology, Institute of Industrial Ecological Sciences, University of Occupational and Environmental Health, 1-1, Iseigaoka, Yahatanishi-ku, Kitakyushu, 807-8555, Japan

Received March 12, 2009

During carcinogenesis, methylation of the C-5 position of cytosines in the promoter region of tumor suppressor genes is often observed. Enzymatic DNA methylation is a widely accepted mechanism for this phenomenon. It is interesting to propose a free radical mechanism for 5-methyldeoxycytidine (m^5dC) production, because the C-5 position of cytosine is an active site for free radical reactions. When deoxycytidine (dC) and cumene hydroperoxide (CuOOH), a tumor promoter and a methyl radical producer, were reacted in the presence of ferrous ion at pH 7.4, the formation of m^5dC was observed. The same reaction also proceeded with *t*-butyl hydroperoxide (BuOOH). The formation of m^5dC was also observed in DNA by the CuOOH treatment. This is the first report of chemical DNA methylation at cytosine C-5 by environmental tumor promoters. We propose here that this reaction is one of the important mechanisms of de novo DNA methylation during carcinogenesis, because methyl radicals are produced by the biotransformation of various endogenous and exogenous compounds.

Introduction

DNA methylation is an important epigenetic mechanism of transcriptional control and plays an essential role in maintaining normal cellular function. During carcinogenesis, the methylation of CpG islands in the promoter regions of tumor suppressor genes occurs, and this can lead to a loss of the gene function or to gene silencing (*1*, *2*). The hypermethylation of the promoter regions of these genes is frequently observed in human cancer (*3*). Therefore, during multistage carcinogenesis, both mutation and hypermethylation can lead to an inactive tumor suppressor gene. It is generally accepted that methylation occurs enzymatically by de novo DNA methyl transferases, such as DNMT3b (*4*). However, the exact mechanisms of hypermethylation, particularly in relation to environmental factors during carcinogenesis, are not clear.

Valinluck and Sowers reported that one possible mechanism of DNA hypermethylation is the formation of inflammation-induced 5-halogenated dC, such as 5-chloro-dC in DNA, which mimics m^5dC and induces inappropriate methylation by the maintenance DNMT1 enzyme within the CpG sequence (*5*). They also reported that a form of inflammation-induced oxidative DNA damage, 5-hydroxymethyldeoxycytidine, prevents DNMT1 methylation within CpG sequences and induces hypomethylation. They proposed that the chemical modification of DNA could cause heritable changes in cytosine methylation patterns, resulting in human tumor formation.

The formation of a mutagenic methyl radical-deoxyguanosine adduct, 8-methyl-2′-deoxyguanosine, has been detected in DNA after a treatment with BuOOH and ferrous ion in vitro or after the administration of 1,2-dimethylhydrazine to rats (*6*–*8*). We proposed a free radical mechanism to produce m^5dC in DNA or the nucleotide pool, because the C-5 position of cytosine is an active site for free radical reactions, in addition to the C-8 of purines and the C-6 position of pyrimidines, on the basis of quantum mechanical calculations (*9*). In this study, environmental tumor promoters, cumene hydroperoxide (CuOOH) and *t*-butyl hydroperoxide (BuOOH), which are known to generate methyl radicals (*10*), were tested for the formation of m^5dC from dC or in DNA.

Experimental Procedures

Materials. Deoxycytidine (dC), calf thymus DNA, poly(dG-dC)·poly(dG-dC), poly(dG)·poly(dC), and 2,2,6,6-tetramethylpiperidine-1-oxyl (TEMPO) were purchased from Sigma-Aldrich (St. Louis, MO). dC was purified by repeated rounds of HPLC (Capcell Pak C18, 5 μm, 10 mm × 250 mm, Shiseido Fine Chemicals, Japan; elution, 5% methanol in water) to remove the small amount of contaminating 5-methyl-dC. α-(4-Pyridyl-1-oxide)-*N*-*tert*-butylnitrone (POBN) was a product of Tokyo Chemical Industry Co., Ltd. (Tokyo, Japan). CuOOH (80% solution) was a product of Lancaster (Morecambe, England). BuOOH (70% solution) and ferrous sulfate ($FeSO_4·7H_2O$) were purchased from Wako Pure Chemical Industries, Ltd. (Osaka, Japan). The $FeSO_4$ solution (100 mM) was prepared just before use for reactions. The anti-5-methyl-dC monoclonal antibody was a gift from Dr. Kazuaki Watanabe, Toray Research Center (Kamakura, Japan) (*11*).

Reaction of dC with CuOOH/Fe^{2+} and Analysis of the Product by HPLC. Detailed reaction conditions are described in the legends to Figures 1−3. After the reaction, the solution was centrifuged, and an aliquot of the supernatant was injected into the HPLC column (YMC-Pak ODS-AM, 4.6 mm × 250 mm, particle size, 5 μm; elution, 5% methanol, 0.9 mL/min) connected with a photodiode array UV detector (Hewlett-Packard 1100 HPLC Detection System).

Reaction of DNA Polymer with CuOOH/Fe^{2+}. Detailed reaction conditions are described in the legend to Figure 4. After

* To whom correspondence should be addressed. Tel: +81-93-691-7469. Fax: +81-93-601-2199. E-mail: h-kasai@med.uoeh-u.ac.jp.

10.1021/tx900099s CCC: $40.75
Published on Web 05/18/2009

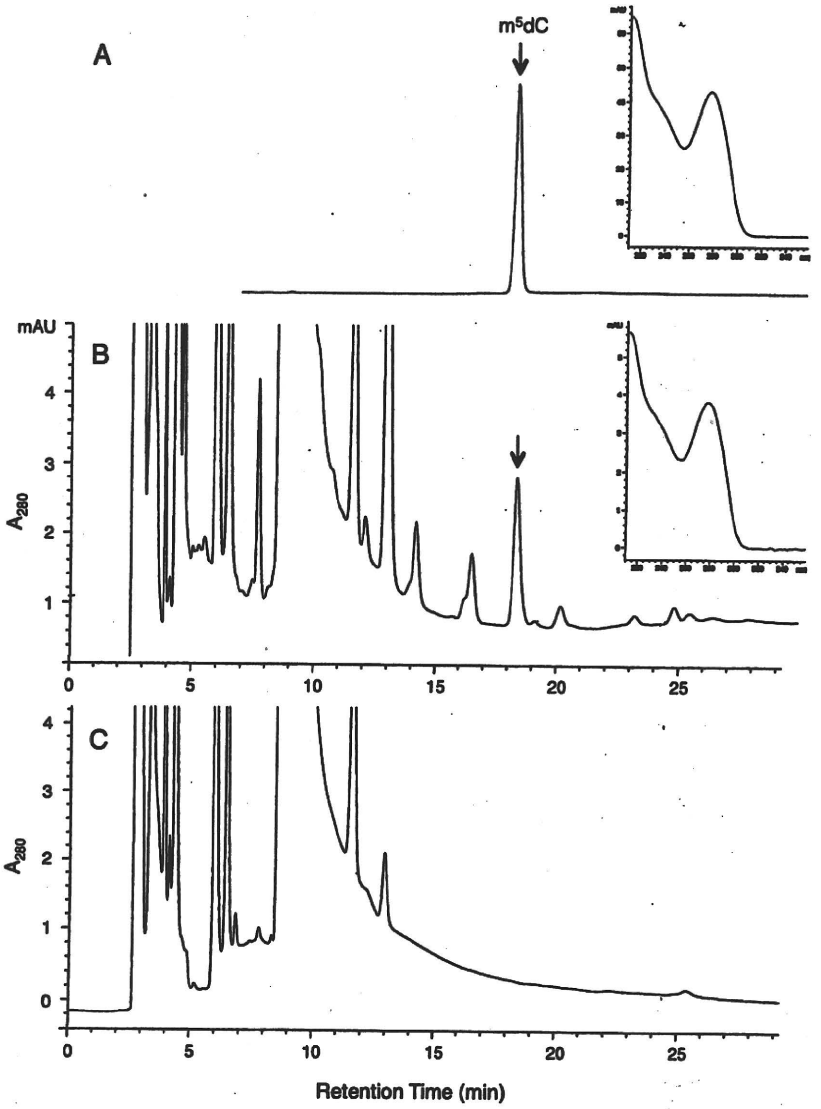

Figure 1. Detection of m^5dC in the reaction mixture of dC, Fe^{2+}, and CuOOH by HPLC. The reaction mixture (final volume, 0.32 mL), containing dC (final concentration, 5.46 mM), $FeSO_4$ (6 mM), and CuOOH (63 mM) in 20 mM phosphate buffer (pH 7.4), was reacted in a sealed plastic tube (tube volume, 2 mL) by vigorous shaking at 20 °C. After a 1 h of reaction, the solution was centrifuged, and an aliquot of the supernatant was injected into the HPLC apparatus. (A) Chromatogram of the m^5dC standard and its UV spectrum (inset), (B) chromatogram of the reaction mixture and UV spectrum of the peak at 18.5 min (inset), and (C) chromatogram of the control reaction mixture without CuOOH.

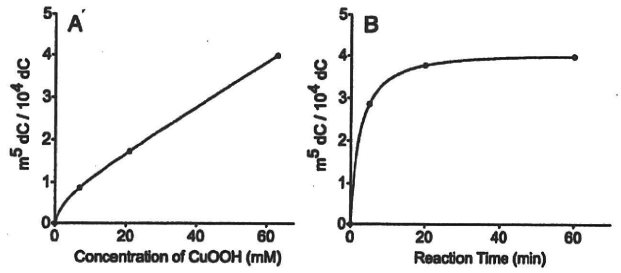

Figure 2. Dose and time dependency of m^5dC formation in the dC/CuOOH/Fe^{2+} reaction. (A) Dose dependency: The reaction conditions were the same as those in Figure 1, except that three different concentrations of CuOOH (7, 21, or 63 mM) were used. Mean values of duplicate experiments are plotted. (B) Time dependency: The reaction conditions were the same as those in Figure 1, except that the reaction was stopped at 5, 20, and 60 min. Mean values of duplicate experiments are plotted.

a 5 min reaction, the reaction mixture was centrifuged, and the supernatant (290 μL) was mixed with 87 μL of 5 M NaCl and 754 μL of cold ethanol and kept at 5 °C to precipitate the DNA. The DNA was recovered, washed with cold ethanol, dried under reduced pressure, and then dissolved in 260 μL of 1 mM EDTA (pH 8.0). For the LC/MS/MS analysis, a 170 μL aliquot of the sample was digested with 14 units of nuclease P1 and 4 units of alkaline phosphatase. For immunodot blot analysis, the DNA solution was centrifuged, and the supernatant was passed through a centrifugal filter device (Amicon Microcon YM-100) to recover the high molecular weight DNA (MW > 100000). The DNA trapped by the filter was dissolved in 150 μL of 1 mM EDTA (pH 8.0).

Detection of m^5dC in DNA by Immunodot Blot Analysis. The immunodot blot analysis was performed by basically the same method as previously reported (*12*). A calf thymus DNA sample (1 mg/mL PBS) was sonicated to obtain fragments of DNA. The DNA solution was then heat-denatured and diluted with 2 M ammonium acetate to an appropriate concentration (1−100 ng/mL). When the oligonucleotide was used, the sonication step was omitted. Single-stranded DNA and oligonucleotides (containing 0.1−10 ng DNA or 50 μg oligonucle-

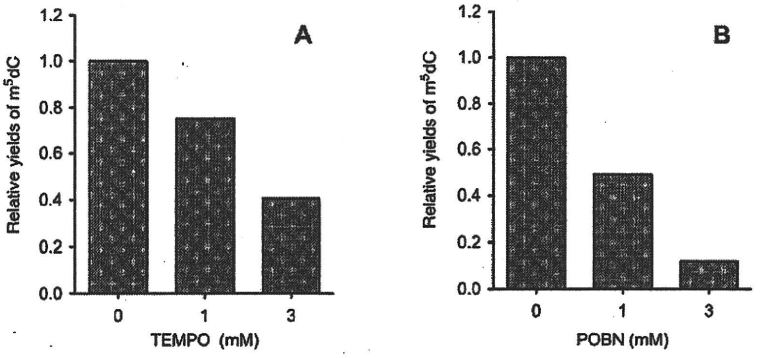

Figure 3. Inhibition of m^5dC formation from dC by TEMPO (A) or POBN (B). The reaction conditions were the same as those in Figure 1, except that the reaction time was 20 min. The reaction was conducted in the presence or absence of TEMPO and POBN. The ratio to the m^5dC yield without TEMPO or POBN (1.0) is shown.

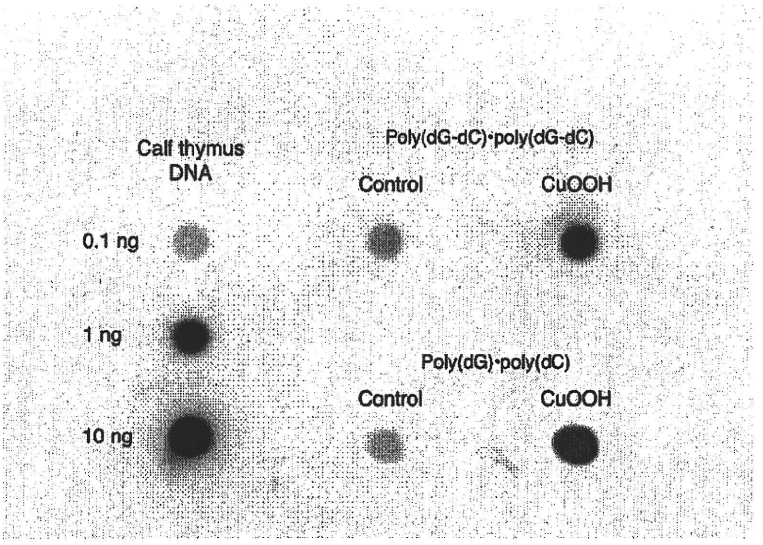

Figure 4. Detection of m^5dC in DNA polymers by an immunodot blot analysis. The reaction mixture (final volume, 0.32 mL) contained poly(dG-dC)·poly(dG-dC) or poly(dG)·poly(dC) (final concentration, 10 A_{260} OD units/mL), $FeSO_4$ (6 mM), and CuOOH (63 mM) in 20 mM phosphate buffer (pH 7.4) and was reacted in a sealed plastic tube (tube volume, 2 mL) by vigorous shaking at 20 °C. After 5 min, the polymers were recovered from the reaction mixture, as described in the Experimental Procedures, and were used for the analysis. As positive controls, m^5dC in various amounts of calf thymus DNA was visualized. As negative controls, DNA polymers without treatment were analyzed.

otide /100 μL sample) were immobilized on a nitrocellulose membrane (0.45 μm, Bio-Rad Laboratories, CA) using a Bio-Dot Microfiltration Apparatus (Bio-Rad Laboratories). The wells were rinsed with 200 μL of 2 M ammonium acetate. The filter was subsequently removed from the support, and the DNA was cross-linked to the nitrocellulose using a Spectrolinker XL 1000 UV (Spectronics Co., NY). The membrane was washed twice for 5 min with PBS-Tween 20 (0.05%) (PBS-T) containing 2% ECL Advance Blocking Agent (GE Healthcare, Buckinghamshire, United Kingdom) (blocking solution). The membrane was then incubated overnight at 4 °C with the blocking solution containing an anti-m^5dC monoclonal antibody (1.3 μg/mL) (*11*). The membrane was washed three times with PBS-T and was then incubated with the secondary antibody diluted 1:75000 in the blocking solution (ECL Anti-Mouse IgG Horseradish Peroxidase-Linked Species-Specific Whole Antibody, from sheep, GE Healthcare) for 2 h at room temperature. The membrane was washed four times with PBS-T. The enzymatic activity was visualized with an Amersham ECL advance Western blotting detection kit (GE Healthcare). The chemiluminescence output from the membrane was imaged using a CCD imager (Light Capture AE-6972, ATTO, Tokyo, Japan).

LC/MS/MS Analysis. The LC/MS/MS data were acquired on a Waters Micromass Quattro Ultima Pt triple quadrupole mass spectrometer with an ESI source (Waters Corp., Milford, MA). It was operated in the positive ion mode with a potential of 35 V. The desolvation temperature was 350 °C, and the ion source temperature was 120 °C. The collision energy was 11 eV. HPLC was performed using a Waters Alliance 2695 system (Waters Corp.), with a Capcell Pak C18 MG column, 5 μm, 2.0 mm × 250 mm (Shiseido Fine Chemicals, Japan); column temperature, 40 °C; elution, 8% aqueous methanol containing 10 mM ammonium formate; and elution speed, 0.2 mL/min.

Results

Reaction of dC with CuOOH/Fe^{2+}. When dC was reacted with CuOOH in the presence of Fe^{2+} at pH 7.4, the formation of m^5dC was clearly identified by HPLC equipped with a photodiodo array UV detector (Figure 1). The retention time and the UV spectrum of the reaction product were exactly the same as those of the authentic m^5dC. Its formation was dependent on the concentration of CuOOH (Figure 2A), and the reaction was rather rapid, due to its radical character. The reaction was approximately 70% complete within 5 min (Figure 2B). The methyl radical is produced by the reduction of CuOOH by Fe^{2+}. It is reasonable to speculate that the methyl radical formation rate and the m^5dC formation rate are dependent upon

Table 1. Yield of m^5dC from dC by BuOOH/Fe^{2+} Treatment[a]

reaction condition		yield of $m^5dC/10^4dC$
1 N H_2SO_4		25.4
0.35 N H_2SO_4		21.3
pH 4.5	air	6.01
	N_2	5.94
pH 7.4	air	1.76
	N_2	2.19

[a] dC (final concentration, 5.46 mM) and $FeSO_4$ (4 mM) were mixed in 0.32 mL of 20 mM sodium acetate buffer (pH 4.5), 20 mM phosphate buffer (pH 7.4), or in H_2SO_4 solutions (0.35 or 1 N), and the reaction was started by adding BuOOH (final concentration, 16 mM) in a sealed plastic tube (tube volume, 2 mL) by vigorous shaking at 20 °C. In some experiments, the oxygen in the solution was removed by flushing with nitrogen gas before starting the reactions. After a 30 min reaction, the solution was centrifuged, and an aliquot of the supernatant was injected into the HPLC apparatus. For the reactions in H_2SO_4 solutions, the supernatant was neutralized with 5 M NaOH, and then, an aliquot was injected into the HPLC apparatus.

the CuOOH concentration with the same concentration of Fe^{2+}. When a radical scavenger, TEMPO or POBN, was added to the reaction mixture at a concentration up to 3 mM, the m^5dC formation was inhibited (Figure 3). It should be mentioned that POBN is an efficient trapping agent for methyl radicals (*8*), while TEMPO, in addition to combining with methyl radicals, oxidizes Fe^{2+}, which is an important factor to produce methyl radicals (*13*). From these results, it can be concluded that this reaction proceeds via a free radical mechanism, probably via a methyl radical.

Reaction of dC with BuOOH/Fe^{2+}. The formation of m^5dC from dC was also observed after a reaction with BuOOH/Fe^{2+} at pH 7.4 (Table 1). Acidification of the reaction conditions increased the yield of m^5dC. When oxygen was removed from the reaction mixture at pH 7.4, the yield increased by 25%. The methyl radicals produced in the reaction may partly react with oxygen under aerobic conditions to form methyl peroxy radicals and then further decompose to formaldehyde.

Reaction of DNA Polymers with CuOOH/Fe^{2+}. After a double-stranded homopolymer, poly(dG)·poly(dC), or an alternating copolymer, poly(dG-dC)·poly(dG-dC), was reacted with CuOOH in the presence of Fe^{2+} at pH 7.4, the formation of m^5dC was examined by an immunodot blot analysis. The formation of m^5dC was clearly detected in both DNA polymers after the treatment (Figure 4). As a positive control, we analyzed 0.1, 1, and 10 ng of calf thymus DNA, because it contains 1.39 mol % m^5dC. The chemiluminescence intensity increased depending upon the calf thymus DNA concentration. The control DNA polymers without treatment also showed weak chemiluminescence. This means that commercial DNA polymers contain a small amount of m^5dC. We considered the immunodot blot analysis to be semiquantitative; therefore, the exact amount of m^5dC in the reaction mixture was analyzed by the LC/MS/MS method.

Confirmation of m^5dC Formation in the Reaction Mixtures by LC/MS/MS Analysis. In the LC/MS analysis, the standard m^5dC exhibited an MH^+ ion at *m/z* 242, and product ion analysis from *m/z* 242 with 11 eV revealed a fragment BH_2^+ ion at *m/z* 126 that is formed by the loss of 2′-deoxyribose (Figure 5). Therefore, the m^5dC in the reaction mixture was analyzed by LC/MS/MS, by monitoring the *m/z* 242 → 126 transition. In Figure 6, chromatograms of the LC/MS/MS analysis of standard m^5dC (A), dC-BuOOH/ Fe^{2+}(B), and DNA polymer- CuOOH/ Fe^{2+}(C) are shown. In both the dC- and the polymer DNA-product analysis, a 242 → 126 transition peak

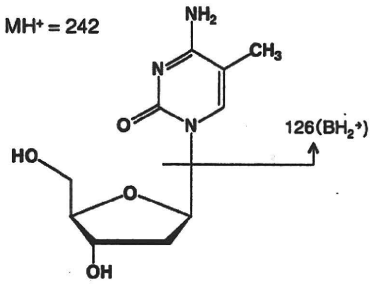

Figure 5. MH^+ ion of m^5dC and the product ion BH_2^+ in the LC/MS/MS analysis.

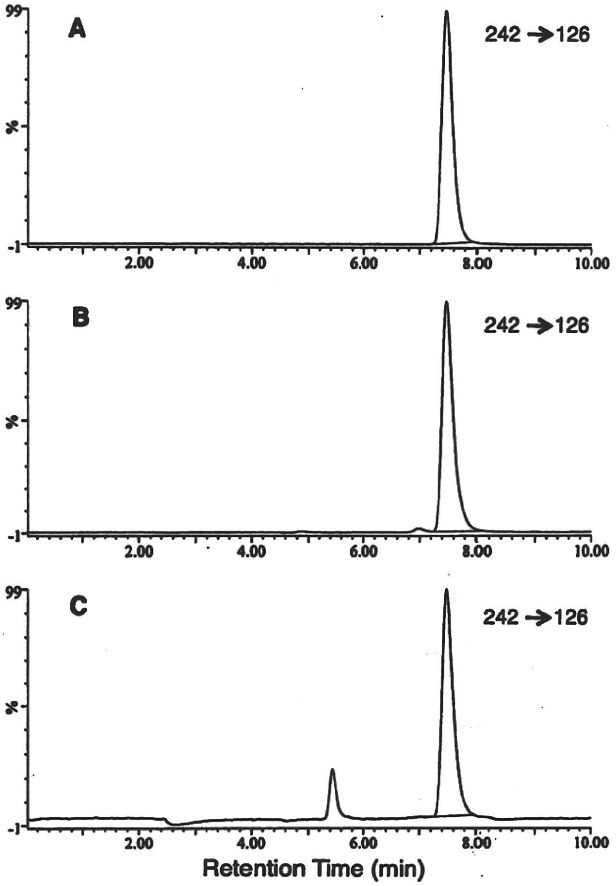

Figure 6. LC/MS/MS analysis of the reaction products. (A) Standard m^5dC (356 ng/mL), (B) dC-BuOOH/Fe^{2+} reaction mixture (reaction conditions were the same as in Table 1, at pH 7.4 and with air), and (C) hydrolysate of poly(dG-dC)·poly(dG-dC)-CuOOH/Fe^{2+} reaction product (reaction conditions were the same as in Figure 4). A 2 μL portion of each sample was injected. The transition *m/z* 242 → 126 was monitored.

appeared at 7.47 min, which is the same retention time as that of authentic m^5dC.

On the basis of the LC/MS/MS analysis, the yield of m^5dC in the dC-BuOOH/Fe^{2+} reaction was calculated to be $1.97/10^4$ dC, which is comparable to that estimated by HPLC-UV ($1.76/10^4$ dC, see Table 1). On the other hand, the yield of m^5dC in the DNA polymer/CuOOH/Fe^{2+} reaction was $2.97/10^5$ dC, while that from dC with the same reaction condition was $2.85/10^4$ dC (see Figure 2B). Therefore, the yield of m^5dC formation is 10-fold lower in DNA than in the dC monomer.

Discussion

A generally accepted concept of the mechanism of de novo DNA methylation during carcinogenesis is the enzymatic

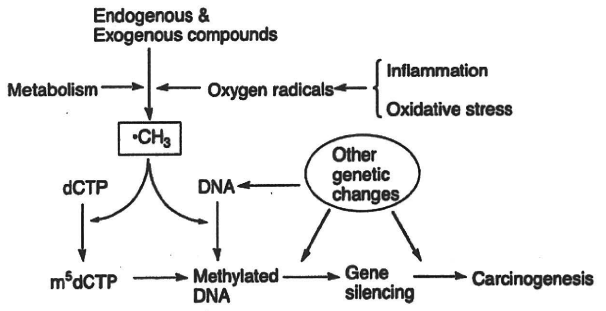

Figure 7. Hypothetical formation of m^5dC in nucleotides and DNA via methyl radicals.

reaction by DNMT3b, using *S*-adenosylmethionine as the methyl donor. Correlations between DNMT3b polymorphisms and neoplastic outcomes have been reported (*14, 15*). It was also reported that tumor suppressor gene inactivation during cadmium-induced transformation is correlated with the overexpression of the de novo DNA methyltransferase DNMT3b (*16*). In the present study, a free radical mechanism to produce m^5dC in DNA or the nucleotide pool was proposed, because the C-5 position of cytosine is an active site for free radical reactions. We observed the methylation of the C-5 position of cytosine in the nucleoside and DNA by the tumor promoters, BuOOH and CuOOH, in the presence of Fe^{2+} via a free radical mechanism. The generation of methyl radicals from organic hydroperoxide tumor promoters in vitro and in isolated mouse keratinocytes has been previously characterized by ESR (*10*). In addition to these chemicals, the generation of methyl radicals by the chemical and biological transformation of various carcinogens has been characterized in vitro and in vivo. For instance, methyl hydrazine derivatives, such as 1,2-dimethylhydrazine (*17*) and procarbazine (*18*), are metabolized to methyl radicals. Acetaldehyde, which is an important human carcinogen related to smoking, drinking, and inflammation (*19, 20*), generates methyl radicals upon treatment with xanthine oxidase (*21*), peroxynitrite (*22*), and iron (II)/hydrogen peroxide (*22*). The amino acid methionine produces a methyl radical upon γ-irradiation (*23*) and by the treatment of its sulfoxide derivative with peroxynitrite (*24*).

During tumor promotion in mouse skin by cigarette smoke condensate, hypermethylation in the promoter regions of the HoxA5, p16, and MGMT genes and their inactivation are important mechanisms of clonal expansion (*25*). Cigarette smoke is known to generate oxygen and carbon radicals (*26*). CuOOH treatment also reportedly induces malignant carcinomas in DMBA, TPA-carcinogenesis experiments with mice (*27, 28*). Therefore, DNA hypermethylation is an important mechanism of tumor promotion and progression.

Our results indicate that the formation of m^5dC in DNA does not seem to be specific to the CpG sequence, and the yield is rather low. Even if the methylation is a rare reaction, the m^5dC thus produced in DNA is not repaired, and its formation in CpG sequences would accumulate during continuous cell divisions by the maintenance DNA methyltransferase, DNMT1. When these modifications occur by chance in the promoter sequences of tumor suppressor genes, these cells will acquire a growth advantage over the surrounding cells, which will be further accelerated with other genetic changes.

It is interesting to speculate that m^5dCTP is formed from dCTP by methyl radicals in the nucleotide pool and then is incorporated into DNA (Figure 7), because we found that the yield of m^5dC as the monomer is much higher than that in DNA in the present study. It has been reported that m^5dCTP introduced into cultured CHO V-79 cells by electroporation is incorporated into DNA and induces gene silencing (*29*).

In conclusion, we found the methyl radical mediated formation of m^5dC from dC or in DNA, by a treatment with CuOOH or BuOOH in the presence of ferrous ion at pH 7.4. We have extended our finding to the following hypothesis. Methyl radicals are produced from the metabolism of carcinogens or from endogenous compounds attacked by oxidants generated by inflammation, ionizing radiation, and other oxidative stresses, and they modify dCTP and DNA to form m^5dC (Figure 7). The accumulation of this chemical modification may be one of the mechanisms of epigenetic change to induce gene silencing and carcinogenesis.

Acknowledgment. This work was supported by Grants-in-Aid from the Ministry of Health, Labor and Welfare of Japan.

References

(1) Feinberg, A. P., and Tycko, B. (2004) The history of cancer epigenetics. *Nat. Rev. Cancer 4*, 43–153.
(2) Herman, J. G., and Baylin, S. B. (2003) Gene silencing in cancer in association with promoter hypermethylation. *N. Engl. J. Med. 349*, 2042–2054.
(3) Esteller, M., Corn, P. G., Baylin, S. B., and Herman, J. G. (2001) A gene hypermethylation profile of human cancer. *Cancer Res. 61*, 3225–3229.
(4) Okano, M., Xie, S., and Li, E. (1998) Cloning and characterization of a family of novel mammalian DNA (cytosine5) methyltransferases. *Nat. Genet. 19*, 219–220.
(5) Valinluck, V., and Sowers, L. C. (2007) Endogenous cytosine damage products alter the site selectivity of human DNA maintenance methyltransferase DNMT1. *Cancer Res. 67*, 946–950.
(6) Gasparutto, D., Dherin, C., Boiteux, S, and Cadet, J. (2002) Excision of 8-methylguanine site-specifically incorporated into oligonucleotide substrates by the AlkA protein of *Escherichia coli*. *DNA Repair 1*, 437–447.
(7) Hix, S., Morais, M. D. S., and Augusto, O. (1995) DNA methylation by tert-butylhydroperoxide-iron(II). *Free Radical Biol. Med. 19*, 293–301.
(8) Netto, L. E. S., RamaKrishna, N. V. S., Kolar, C., Cavalier, E. L., Rogan, E. G., Lawson, T. A., and Augusto, O. (1992) Identification of C8-methylguanine in the hydrolysates of DNA from rats administered 1,2-dimethylhydrazine, evidence for in vivo DNA alkylation by methyl radicals. *J. Biol. Chem. 267*, 21524–21527.
(9) Kochetkov, N. K., Budovskii, E. I., Sverdlov, E. D., Simukova, N. A., Turchinskii, M. F., and Shibaev, V. N. (1971) *Organic Chemistry of Nucleic Acid, Part A*, pp 166−171, Plenum Press, London and New York.
(10) Taffe, B. G., Takahashi, N., Kensler, T. W., and Mason, R. P. (1987) Generation of free radicals from organic hydroperoxide tumor promoters in isolated mouse keratinocytes, Formation of alkyl and alkoxyl radicals from *tert*-butyl hydroperoxide and cumene hydroperoxide. *J. Biol. Chem. 262*, 12143–12149.
(11) Sato, K., Shimode, Y., Hirokawa, M., Ueda, Y., and Katsuda, S. (2008) Thyroid adenomatous nodule with bizarre nuclei: A case report and mutation analysis of the p53 gene. *Pathol. Res. Pract. 204*, 191–195.
(12) Leuratti, C., Singh, R., Lagneau, C., Farmer, P. B., Plastaras, J. P., Marnett, L. J., and Shuker, D. E. (1998) Determination of malondialdehyde-induced DNA damage in human tissues using an immunoslot blot assay. *Carcinogenesis 19*, 1919–1924.
(13) Bar-On, P., Mohsen, M., Zhang, R., Feigin, E., Chevion, M., and Samuni, A. (1999) Kinetics of nitroxide reaction with iron(II). *J. Am. Chem. Soc. 121*, 8070–8073.
(14) Singal, R., Das, P. M., Manoharan, M., Reis, I. M., and Schlesselman, J. J. (2005) Polymorphisms in the DNA methyltransferase 3b gene and prostate cancer risk. *Oncol. Rep. 14*, 569–573.
(15) Lee, S. J., Jeon, H. S., Jang, J. S., Park, S. H., Lee, G. Y., Lee, B. H., Kim, C. H., Kang, Y. M., Lee, W. K., Kam, S., Park, R. W., Kim, I. S., Cho, Y. L., Jung, T. H., and Park, J. Y. (2005) DNMT3B polymorphysms and risk of primary lung cancer. *Carcinogenesis 26*, 403–409.
(16) Benbrahim-Talla, L., Waterland, R. A., Dill, A. L., Webber, M. M., and Waalkes, M. P. (2007) Tumor suppressor gene inactivation during cadmium-induced malignant transformation of human prostate cells correlates with overexpression of *de novo* DNA methyltransferase. *Environ. Health Perspect. 115*, 1454–1459.

(17) Augusto, O., Du Plessis, L. R., and Weingrill, C. L. V. (1985) Spin-trapping of methyl radical in the oxidative metabolism of 1,2-dimethylhydrazine. *Biochem. Biophys. Res. Commun. 110*, 625–631.
(18) Goria-Gatti, L., Iannone, A., Tomasi, A., Poli, G., and Albano, E. (1992) In vitro and in vivo evidence for the formation of methyl radical from procarbazine: a spin-trapping study. *Carcinogenesis 13*, 799–805.
(19) Salaspuro, V., and Salaspuro, M. (2004) Synergistic effect of alcohol drinking and smoking on in vivo acetaldehyde concentration in saliva. *Int. J. Cancer 111*, 480–483.
(20) Matsuse, H, Fukushima, C, Shimoda, T, Sadahiro, A, and Kohno, S. (2007) Effects of acetaldehyde on human airway constriction and inflammation. *Novartis Found Symp. 285*, 97–106.
(21) Nakao, L. S., Kadiiska, M. B., Mason, R. P., Grijalba, M. T., and Augusto, O. (2000) Metabolism of acetaldehyde to methyl and acetyl radicals: in vitro and in vivo electron paramagnetic resonance spin-trapping studies. *Free Radical Biol. Med. 29*, 721–729.
(22) Nakao, L. S., Ouchi, D., and Augusto, O. (1999) Oxidation of acetaldehyde by peroxynitrite and hydrogen peroxide/iron(II). Production of acetate, formate, and methyl radicals. *Chem. Res. Toxicol. 12*, 1010–1018.
(23) Makino, K. (1979) Studies on spin-trapped radicals in γ- irradiated aqueous solutions of DL-methionine by high performance liquid chromatography and ESR spectroscopy. *J. Phys. Chem. 83*, 2520–2523.
(24) Nakao, L. S., Iwai, L. K., Kalil, J., and Augusto, O. (2003) Radical production from free and peptide-bound methionine sulfoxide oxidation by peroxynitrite and hydrogen peroxide/iron(II). *FEBS Lett. 547*, 87–91.
(25) Watson, R. E., Curtin, G. M., Hellmann, G. M., Doolittle, D. J., and GoodmanJ, I. (2004) Increased DNA methylation in the HoxA5 promoter region correlates with decreased expression of the gene during tumor promotion. *Mol. Carcinog. 41*, 54–66.
(26) Church, D. F., and Pryor, W. A. (1985) Free-radical chemistry of cigarette smoke and its toxicological implications. *Environ. Health Perspect. 64*, 111–126.
(27) Shvedova, A. A., Kisin, E. R., Murray, A. R., Kommineni, C., Vallyathan, V., and Castranova, V. (2004) Pro/antioxidant status in murine skin following topical exposure to cumene hydroperoxide throughout the ontogeny of skin cancer. *Biochemistry (Moscow) 69*, 23–31.
(28) Murray, A. R., Kisin, E. R., Kommineni, C., Vallyathan, V., Castranova, V., and Shvedova, A. A. (2007) Pro/antioxidant status and AP-1 transcription factor in mouse skin following topical exposure to cumene hydroperoxide. *Carcinogenesis 28*, 1582–1588.
(29) Holliday, R., and Ho, T. (1991) Gene silencing in mammalian cells by uptake of 5-methyl deoxycytidine-5′-triphosphate. *Somat. Cell Mol. Genet. 17*, 537–542.

TX900099S

Chem. Res. Toxicol. **2009,** *22,* 984–989

DNA Methylation at the C-5 Position of Cytosine by Methyl Radicals: A Possible Role for Epigenetic Change during Carcinogenesis by Environmental Agents

Hiroshi Kasai* and Kazuaki Kawai

Department of Environmental Oncology, Institute of Industrial Ecological Sciences, University of Occupational and Environmental Health, 1-1, Iseigaoka, Yahatanishi-ku, Kitakyushu, 807-8555, Japan

Received March 12, 2009

During carcinogenesis, methylation of the C-5 position of cytosines in the promoter region of tumor suppressor genes is often observed. Enzymatic DNA methylation is a widely accepted mechanism for this phenomenon. It is interesting to propose a free radical mechanism for 5-methyldeoxycytidine (m^5dC) production, because the C-5 position of cytosine is an active site for free radical reactions. When deoxycytidine (dC) and cumene hydroperoxide (CuOOH), a tumor promoter and a methyl radical producer, were reacted in the presence of ferrous ion at pH 7.4, the formation of m^5dC was observed. The same reaction also proceeded with *t*-butyl hydroperoxide (BuOOH). The formation of m^5dC was also observed in DNA by the CuOOH treatment. This is the first report of chemical DNA methylation at cytosine C-5 by environmental tumor promoters. We propose here that this reaction is one of the important mechanisms of de novo DNA methylation during carcinogenesis, because methyl radicals are produced by the biotransformation of various endogenous and exogenous compounds.

Introduction

DNA methylation is an important epigenetic mechanism of transcriptional control and plays an essential role in maintaining normal cellular function. During carcinogenesis, the methylation of CpG islands in the promoter regions of tumor suppressor genes occurs, and this can lead to a loss of the gene function or to gene silencing (*1*, *2*). The hypermethylation of the promoter regions of these genes is frequently observed in human cancer (*3*). Therefore, during multistage carcinogenesis, both mutation and hypermethylation can lead to an inactive tumor suppressor gene. It is generally accepted that methylation occurs enzymatically by de novo DNA methyl transferases, such as DNMT3b (*4*). However, the exact mechanisms of hypermethylation, particularly in relation to environmental factors during carcinogenesis, are not clear.

Valinluck and Sowers reported that one possible mechanism of DNA hypermethylation is the formation of inflammation-induced 5-halogenated dC, such as 5-chloro-dC in DNA, which mimics m^5dC and induces inappropriate methylation by the maintenance DNMT1 enzyme within the CpG sequence (*5*). They also reported that a form of inflammation-induced oxidative DNA damage, 5-hydroxymethyldeoxycytidine, prevents DNMT1 methylation within CpG sequences and induces hypomethylation. They proposed that the chemical modification of DNA could cause heritable changes in cytosine methylation patterns, resulting in human tumor formation.

The formation of a mutagenic methyl radical-deoxyguanosine adduct, 8-methyl-2′-deoxyguanosine, has been detected in DNA after a treatment with BuOOH and ferrous ion in vitro or after the administration of 1,2-dimethylhydrazine to rats (*6*–*8*). We proposed a free radical mechanism to produce m^5dC in DNA or the nucleotide pool, because the C-5 position of cytosine is an active site for free radical reactions, in addition to the C-8 of purines and the C-6 position of pyrimidines, on the basis of quantum mechanical calculations (*9*). In this study, environmental tumor promoters, cumene hydroperoxide (CuOOH) and *t*-butyl hydroperoxide (BuOOH), which are known to generate methyl radicals (*10*), were tested for the formation of m^5dC from dC or in DNA.

Experimental Procedures

Materials. Deoxycytidine (dC), calf thymus DNA, poly(dG-dC)·poly(dG-dC), poly(dG)·poly(dC), and 2,2,6,6-tetramethylpiperidine-1-oxyl (TEMPO) were purchased from Sigma-Aldrich (St. Louis, MO). dC was purified by repeated rounds of HPLC (Capcell Pak C18, 5 μm, 10 mm × 250 mm, Shiseido Fine Chemicals, Japan; elution, 5% methanol in water) to remove the small amount of contaminating 5-methyl-dC. α-(4-Pyridyl-1-oxide)-*N*-*tert*-butylnitrone (POBN) was a product of Tokyo Chemical Industry Co., Ltd. (Tokyo, Japan). CuOOH (80% solution) was a product of Lancaster (Morecambe, England). BuOOH (70% solution) and ferrous sulfate ($FeSO_4·7H_2O$) were purchased from Wako Pure Chemical Industries, Ltd. (Osaka, Japan). The $FeSO_4$ solution (100 mM) was prepared just before use for reactions. The anti-5-methyl-dC monoclonal antibody was a gift from Dr. Kazuaki Watanabe, Toray Research Center (Kamakura, Japan) (*11*).

Reaction of dC with CuOOH/Fe^{2+} and Analysis of the Product by HPLC. Detailed reaction conditions are described in the legends to Figures 1–3. After the reaction, the solution was centrifuged, and an aliquot of the supernatant was injected into the HPLC column (YMC-Pak ODS-AM, 4.6 mm × 250 mm, particle size, 5 μm; elution, 5% methanol, 0.9 mL/min) connected with a photodiode array UV detector (Hewlett-Packard 1100 HPLC Detection System).

Reaction of DNA Polymer with CuOOH/Fe^{2+}. Detailed reaction conditions are described in the legend to Figure 4. After

* To whom correspondence should be addressed. Tel: +81-93-691-7469. Fax: +81-93-601-2199. E-mail: h-kasai@med.uoeh-u.ac.jp.

10.1021/tx900099s CCC: $40.75
Published on Web 05/18/2009

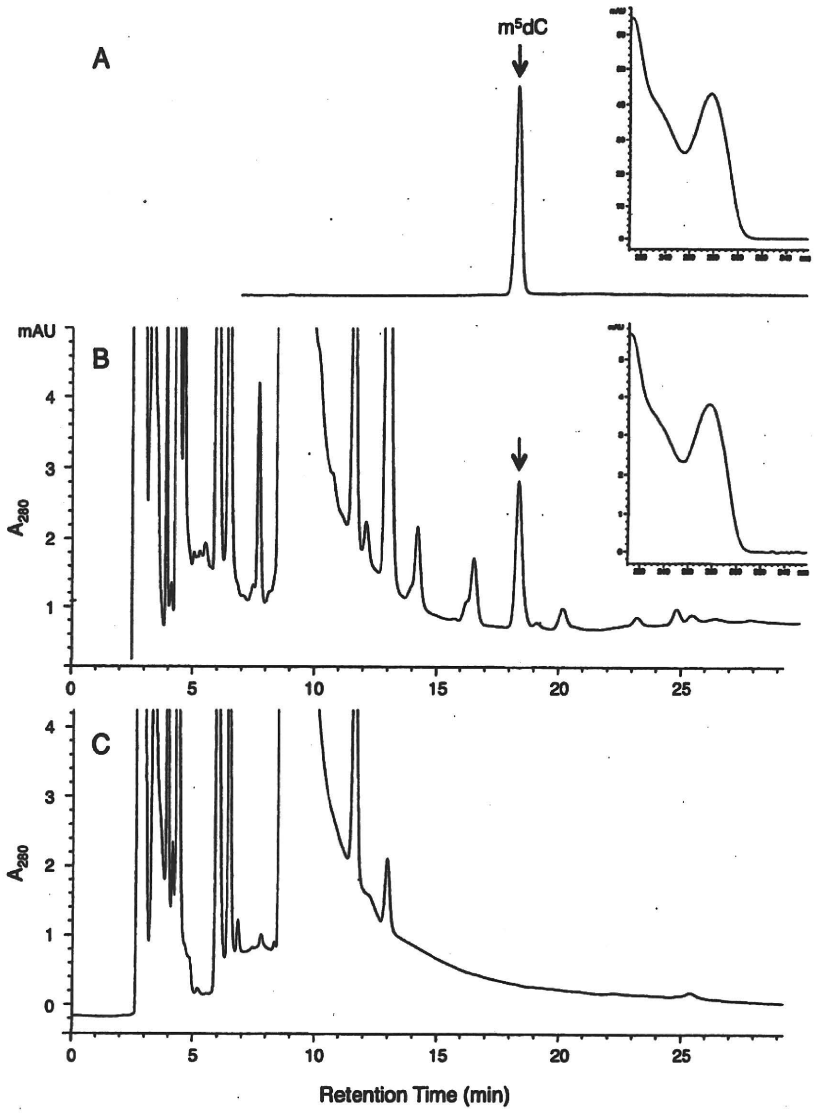

Figure 1. Detection of m^5dC in the reaction mixture of dC, Fe^{2+}, and CuOOH by HPLC. The reaction mixture (final volume, 0.32 mL), containing dC (final concentration, 5.46 mM), $FeSO_4$ (6 mM), and CuOOH (63 mM) in 20 mM phosphate buffer (pH 7.4), was reacted in a sealed plastic tube (tube volume, 2 mL) by vigorous shaking at 20 °C. After a 1 h of reaction, the solution was centrifuged, and an aliquot of the supernatant was injected into the HPLC apparatus. (A) Chromatogram of the m^5dC standard and its UV spectrum (inset), (B) chromatogram of the reaction mixture and UV spectrum of the peak at 18.5 min (inset), and (C) chromatogram of the control reaction mixture without CuOOH.

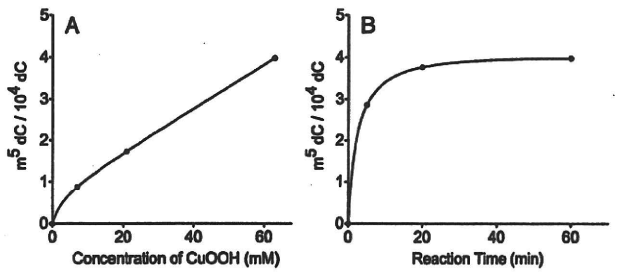

Figure 2. Dose and time dependency of m^5dC formation in the dC/CuOOH/Fe^{2+} reaction. (A) Dose dependency: The reaction conditions were the same as those in Figure 1, except that three different concentrations of CuOOH (7, 21, or 63 mM) were used. Mean values of duplicate experiments are plotted. (B) Time dependency: The reaction conditions were the same as those in Figure 1, except that the reaction was stopped at 5, 20, and 60 min. Mean values of duplicate experiments are plotted.

a 5 min reaction, the reaction mixture was centrifuged, and the supernatant (290 μL) was mixed with 87 μL of 5 M NaCl and 754 μL of cold ethanol and kept at 5 °C to precipitate the DNA. The DNA was recovered, washed with cold ethanol, dried under reduced pressure, and then dissolved in 260 μL of 1 mM EDTA (pH 8.0). For the LC/MS/MS analysis, a 170 μL aliquot of the sample was digested with 14 units of nuclease P1 and 4 units of alkaline phosphatase. For immunodot blot analysis, the DNA solution was centrifuged, and the supernatant was passed through a centrifugal filter device (Amicon Microcon YM-100) to recover the high molecular weight DNA (MW > 100000). The DNA trapped by the filter was dissolved in 150 μL of 1 mM EDTA (pH 8.0).

Detection of m^5dC in DNA by Immunodot Blot Analysis. The immunodot blot analysis was performed by basically the same method as previously reported (*12*). A calf thymus DNA sample (1 mg/mL PBS) was sonicated to obtain fragments of DNA. The DNA solution was then heat-denatured and diluted with 2 M ammonium acetate to an appropriate concentration (1−100 ng/mL). When the oligonucleotide was used, the sonication step was omitted. Single-stranded DNA and oligonucleotides (containing 0.1−10 ng DNA or 50 μg oligonucle-

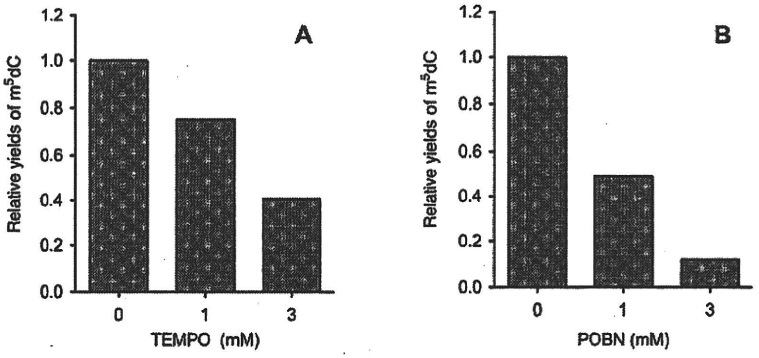

Figure 3. Inhibition of m^{5}dC formation from dC by TEMPO (A) or POBN (B). The reaction conditions were the same as those in Figure 1, except that the reaction time was 20 min. The reaction was conducted in the presence or absence of TEMPO and POBN. The ratio to the m^{5}dC yield without TEMPO or POBN (1.0) is shown.

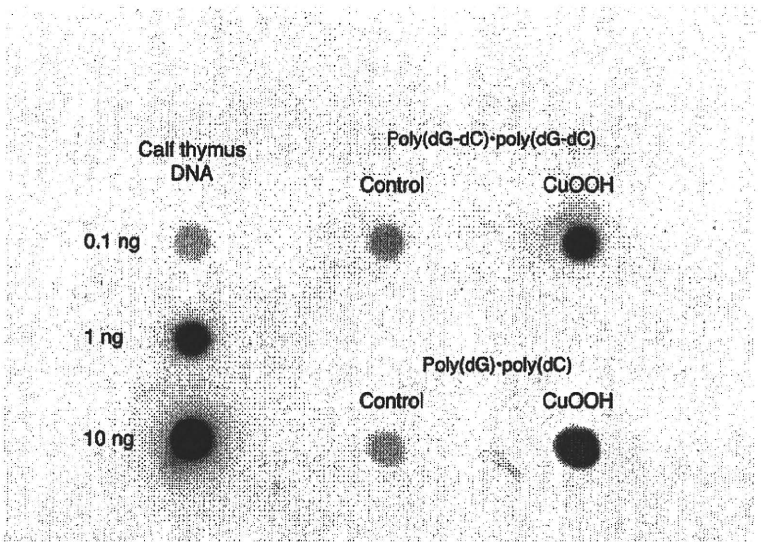

Figure 4. Detection of m^{5}dC in DNA polymers by an immunodot blot analysis. The reaction mixture (final volume, 0.32 mL) contained poly(dG-dC)•poly(dG-dC) or poly(dG)•poly(dC) (final concentration, 10 A_{260} OD units/mL), $FeSO_4$ (6 mM), and CuOOH (63 mM) in 20 mM phosphate buffer (pH 7.4) and was reacted in a sealed plastic tube (tube volume, 2 mL) by vigorous shaking at 20 °C. After 5 min, the polymers were recovered from the reaction mixture, as described in the Experimental Procedures, and were used for the analysis. As positive controls, m^{5}dC in various amounts of calf thymus DNA was visualized. As negative controls, DNA polymers without treatment were analyzed.

otide /100 μL sample) were immobilized on a nitrocellulose membrane (0.45 μm, Bio-Rad Laboratories, CA) using a Bio-Dot Microfiltration Apparatus (Bio-Rad Laboratories). The wells were rinsed with 200 μL of 2 M ammonium acetate. The filter was subsequently removed from the support, and the DNA was cross-linked to the nitrocellulose using a Spectrolinker XL 1000 UV (Spectronics Co., NY). The membrane was washed twice for 5 min with PBS-Tween 20 (0.05%) (PBS-T) containing 2% ECL Advance Blocking Agent (GE Healthcare, Buckinghamshire, United Kingdom) (blocking solution). The membrane was then incubated overnight at 4 °C with the blocking solution containing an anti-m^{5}dC monoclonal antibody (1.3 μg/mL) (*11*). The membrane was washed three times with PBS-T and was then incubated with the secondary antibody diluted 1:75000 in the blocking solution (ECL Anti-Mouse IgG Horseradish Peroxidase-Linked Species-Specific Whole Antibody, from sheep, GE Healthcare) for 2 h at room temperature. The membrane was washed four times with PBS-T. The enzymatic activity was visualized with an Amersham ECL advance Western blotting detection kit (GE Healthcare). The chemiluminescence output from the membrane was imaged using a CCD imager (Light Capture AE-6972, ATTO, Tokyo, Japan).

LC/MS/MS Analysis. The LC/MS/MS data were acquired on a Waters Micromass Quattro Ultima Pt triple quadrupole mass spectrometer with an ESI source (Waters Corp., Milford, MA). It was operated in the positive ion mode with a potential of 35 V. The desolvation temperature was 350 °C, and the ion source temperature was 120 °C. The collision energy was 11 eV. HPLC was performed using a Waters Alliance 2695 system (Waters Corp.), with a Capcell Pak C18 MG column, 5 μm, 2.0 mm × 250 mm (Shiseido Fine Chemicals, Japan); column temperature, 40 °C; elution, 8% aqueous methanol containing 10 mM ammonium formate; and elution speed, 0.2 mL/min.

Results

Reaction of dC with CuOOH/Fe^{2+}. When dC was reacted with CuOOH in the presence of Fe^{2+} at pH 7.4, the formation of m^{5}dC was clearly identified by HPLC equipped with a photodiodo array UV detector (Figure 1). The retention time and the UV spectrum of the reaction product were exactly the same as those of the authentic m^{5}dC. Its formation was dependent on the concentration of CuOOH (Figure 2A), and the reaction was rather rapid, due to its radical character. The reaction was approximately 70% complete within 5 min (Figure 2B). The methyl radical is produced by the reduction of CuOOH by Fe^{2+}. It is reasonable to speculate that the methyl radical formation rate and the m^{5}dC formation rate are dependent upon